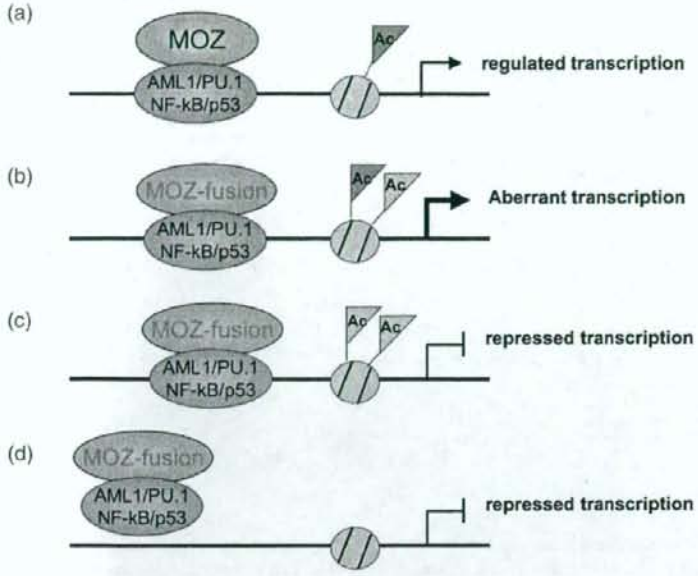

Fig. 4. Models of aberrant transcription in acute myeloid leukemia (AML) with monocytic leukemia zinc finger protein (MOZ) fusion genes. (a) MOZ maintains appropriate chromatin status to regulate target gene expression and hematopoiesis. (b) Constitutively active transcription is induced by MOZ fusion proteins through unusual chromatin status such as hyper-acetylation in leukemia. (c) MOZ fusions induce unusual chromatin status and then down-regulate target gene expression. (d) MOZ fusions deplete transcription factors and/or their coactovators, and then down-regulate target gene expression. Ac, acetylation.

monocytic leukemia, MOZ fuses with CBP, p300 or TIF2, all of which are involved in histone modification. MOZ fusion proteins positively and negatively affect transcription of MOZ target genes to induce leukemia. Further investigation is needed into the functions of MOZ and MOZ fusion genes in hematopoiesis and leukemogenesis in order to develop improved AML therapeutics.

Acknowledgments

This work was supported in part by Grants-in-Aid for Scientific Research from the Ministry of Health, Labor and Welfare and from the Ministry of Education, Culture, Sports, Science, and Technology, and by the Program for Promotion of Fundamental Studies from the National Institute of Biomedical Innovation of Japan.

References

1 Look AT. Oncogenic transcription factors in the human acute leukemias. *Science* 1997; 278: 1059–64.
2 Mrozek K, Heinonen K, Bloomfield CD. Clinical importance of cytogenetics in acute myeloid leukaemia. *Best Pract Res Clin Haematol* 2001; 14: 19–47.
3 Scandura JM, Boccuni P, Cammenga J, Nimer SD. Transcription factor fusions in acute leukemia: variations on a theme. *Oncogene* 2002; 21: 3422–44.
4 Di Croce L. Chromatin modifying activity of leukaemia associated fusion proteins. *Hum Mol Genet* 2005; 14 (Spec 1): R77–84.
5 Kitabayashi I, Aikawa Y, Nguyen LA, Yokoyama A, Ohki M. Activation of AML1-mediated transcription by MOZ and inhibition by the MOZ–CBP fusion protein. *Embo J* 2001; 20: 7184–96.
6 Champagne N, Pelletier N, Yang XJ. The monocytic leukemia zinc finger protein MOZ is a histone acetyltransferase. *Oncogene* 2001; 20: 404–9.
7 Thomas T, Corcoran LM, Gugasyan R *et al.* Monocytic leukemia zinc finger protein is essential for the development of long-term reconstituting hematopoietic stem cells. *Genes Dev* 2006; 20: 1175–86.
8 Katsumoto T, Aikawa Y, Iwama A *et al.* MOZ is essential for maintenance of hematopoietic stem cells. *Genes Dev* 2006; 20: 1321–30.
9 Deguchi K, Ayton PM, Carapeti M *et al.* MOZ–TIF2-induced acute myeloid leukemia requires the MOZ nucleosome binding motif and TIF2-mediated recruitment of CBP. *Cancer Cell* 2003; 3: 259–71.
10 Huntly BJ, Gilliland DG. Leukaemia stem cells and the evolution of cancer-stem-cell research. *Nat Rev Cancer* 2005; 5: 311–21.
11 Borrow J, Stanton VP Jr, Andresen JM *et al.* The translocation t(8;16) (p11;p13) of acute myeloid leukaemia fuses a putative acetyltransferase to the CREB-binding protein. *Nat Genet* 1996; 14: 33–41.
12 Chaffanet M, Gressin L, Preudhomme C, Soenen-Cornu V, Birnbaum D, Pebusque MJ. MOZ is fused to p300 in an acute monocytic leukemia with t(8;22). *Genes Chromosomes Cancer* 2000; 28: 138–44.
13 Kitabayashi I, Aikawa Y, Yokoyama A *et al.* Fusion of MOZ and p300 histone acetyltransferases in acute monocytic leukemia with a t(8;22) (p11;q13) chromosome translocation. *Leukemia* 2001; 15: 89–94.
14 Carapeti M, Aguiar RC, Goldman JM, Cross NC. A novel fusion between MOZ and the nuclear receptor coactivator TIF2 in acute myeloid leukemia. *Blood* 1998; 91: 3127–33.
15 Liang J, Prouty L, Williams BJ, Dayton MA, Blanchard KL. Acute mixed lineage leukemia with an inv (8) (p11q13) resulting in fusion of the genes for MOZ and TIF2. *Blood* 1998; 92: 2118–22.
16 Esteyries S, Perot C, Adelaide J *et al.* NCOA3, a new fusion partner for MOZ/MYST3 in M5 acute myeloid leukemia. *Leukemia* 2007; 22: 663–5.
17 Imamura T, Kakazu N, Hibi S *et al.* Rearrangement of the MOZ gene in pediatric therapy-related myelodysplastic syndrome with a novel chromosomal translocation t(2;8) (p23;p11). *Genes Chromosomes Cancer* 2003; 36: 413–19.
18 Yang XJ, Ullah M. MOZ and MORF, two large MYSTic HATs in normal and cancer stem cells. *Oncogene* 2007; 26: 5408–19.
19 Thomas T, Voss AK, Chowdhury K, Gruss P. Querkopf, a MYST family histone acetyltransferase, is required for normal cerebral cortex development. *Development* 2000; 127: 2537–48.
20 Panagopoulos I, Fioretos T, Isaksson M *et al.* Fusion of the MORF and CBP genes in acute myeloid leukemia with the t(10;16) (q22;p13). *Hum Mol Genet* 2001; 10: 395–404.
21 Vizmanos JL, Larrayoz MJ, Lahortiga I *et al.* t(10;16) (q22;p13) and MORF–CREBBP fusion is a recurrent event in acute myeloid leukemia. *Genes Chromosomes Cancer* 2003; 36: 402–5.
22 Kojima K, Kaneda K, Yoshida C *et al.* A novel fusion variant of the MORF and CBP genes detected in therapy-related myelodysplastic syndrome with t(10;16) (q22;p13). *Br J Haematol* 2003; 120: 271–3.
23 Moore SD, Herrick SR, Ince TA *et al.* Uterine leiomyomata with t(10;17) disrupt the histone acetyltransferase MORF. *Cancer Res* 2004; 64: 5570–7.
24 Iyer NG, Ozdag H, Caldas C. p300/CBP and cancer. *Oncogene* 2004; 23: 4225–31.
25 Xu J, Li Q. Review of the *in vivo* functions of the p160 steroid receptor coactivator family. *Mol Endocrinol* 2003; 17: 1681–92.
26 Akhtar A, Becker PB. The histone H4 acetyltransferase MOF uses a C2HC zinc finger for substrate recognition. *EMBO Rep* 2001; 2: 113–8.
27 Holbert MA, Sikorski T, Carten J, Snowflack D, Hodawadekar S, Marmorstein R. The human monocytic leukemia zinc finger histone acetyltransferase domain

doi: 10.1111/j.1349-7006.2008.00865.x

contains DNA-binding activity implicated in chromatin targeting. *J Biol Chem* 2007; 282: 36603–13.
28 Struhl K. Histone acetylation and transcriptional regulatory mechanisms. *Genes Dev* 1998; 12: 599–606.
29 Yang XJ. The diverse superfamily of lysine acetyltransferases and their roles in leukemia and other diseases. *Nucl Acids Res* 2004; 32: 959–76.
30 Doyon Y, Cayrou C, Ullah M *et al.* ING tumor suppressor proteins are critical regulators of chromatin acetylation required for genome expression and perpetuation. *Mol Cell* 2006; 21: 51–64.
31 Avvakumov N, Cote J. The MYST family of histone acetyltransferases and their intimate links to cancer. *Oncogene* 2007; 26: 5395–407.
32 Pelletier N, Champagne N, Stifani S, Yang XJ. MOZ and MORF histone acetyltransferases interact with the Runt-domain transcription factor Runx2. *Oncogene* 2002; 21: 2729–40.
33 Chan EM, Chan RJ, Comer EM *et al.* MOZ and MOZ–CBP cooperate with NF-kappaB to activate transcription from NF-kappaB-dependent promoters. *Exp Hematol* 2007; 35: 1782–92.
34 Kitabayashi I, Yokoyama A, Shimizu K, Ohki M. Interaction and functional cooperation of the leukemia-associated factors AML1 and p300 in myeloid cell differentiation. *Embo J* 1998; 17: 2994–3004.
35 Nguyen LA, Pandolfi PP, Aikawa Y, Tagata Y, Ohki M, Kitabayashi I. Physical and functional link of the leukemia-associated factors AML1 and PML. *Blood* 2005; 105: 292–300.
36 Aikawa Y, Nguyen LA, Isono K *et al.* Roles of HIPK1 and HIPK2 in AML1- and p300-dependent transcription, hematopoiesis and blood vessel formation. *Embo J* 2006; 25: 3955–65.
37 Yoshida H, Kitabayashi I. Chromatin regulation by AML1 complex. *Int J Hematol* 2008; 87: 19–24.
38 Bristow CA, Shore P. Transcriptional regulation of the human MIP-1alpha promoter by RUNX1 and MOZ. *Nucl Acids Res* 2003; 31: 2735–44.
39 Ohta K, Ohigashi M, Naganawa A *et al.* Histone acetyltransferase MOZ acts as a co-activator of Nrf2–MafK and induces tumour marker gene expression during hepatocarcinogenesis. *Biochem J* 2007; 402: 559–66.
40 Miller CT, Maves L, Kimmel CB. *moz* regulates Hox expression and pharyngeal segmental identity in zebrafish. *Development* 2004; 131: 2443–61.
41 Crump JG, Swartz ME, Eberhart JK, Kimmel CB. Moz-dependent Hox expression controls segment-specific fate maps of skeletal precursors in the face. *Development* 2006; 133: 2661–9.
42 Camos M, Esteve J, Jares P *et al.* Gene expression profiling of acute myeloid leukemia with translocation t(8;16) (p11;p13) and MYST3–CREBBP rearrangement reveals a distinctive signature with a specific pattern of HOX gene expression. *Cancer Res* 2006; 66: 6947–54.
43 Okuda T, van Deursen J, Hiebert SW, Grosveld G, Downing JR. AML1, the target of multiple chromosomal translocations in human leukemia, is essential for normal fetal liver hematopoiesis. *Cell* 1996; 84: 321–30.
44 Ichikawa M, Asai T, Saito T *et al.* AML-1 is required for megakaryocytic maturation and lymphocytic differentiation, but not for maintenance of hematopoietic stem cells in adult hematopoiesis. *Nat Med* 2004; 10: 299–304.
45 Growney JD, Shigematsu H, Li Z *et al.* Loss of Runx1 perturbs adult hematopoiesis and is associated with a myeloproliferative phenotype. *Blood* 2005; 106: 494–504.
46 Putz G, Rosner A, Nuesslein I, Schmitz N, Buchholz F. AML1 deletion in adult mice causes splenomegaly and lymphomas. *Oncogene* 2006; 25: 929–39.
47 Kim HG, de Guzman CG, Swindle CS *et al.* The ETS family transcription factor PU.1 is necessary for the maintenance of fetal liver hematopoietic stem cells. *Blood* 2004; 104: 3894–900.
48 Iwasaki H, Somoza C, Shigematsu H *et al.* Distinctive and indispensable roles of PU.1 in maintenance of hematopoietic stem cells and their differentiation. *Blood* 2005; 106: 1590–600.
49 Nutt SL, Metcalf D, D'Amico A, Polli M, Wu L. Dynamic regulation of PU.1 expression in multipotent hematopoietic progenitors. *J Exp Med* 2005; 201: 221–31.
50 Rosenbauer F, Wagner K, Kutok JL *et al.* Acute myeloid leukemia induced by graded reduction of a lineage-specific transcription factor, PU. *1 Nat Genet* 2004; 36: 624–30.
51 Stein MI, Zhu J, Emerson SG. Molecular pathways regulating the self-renewal of hematopoietic stem cells. *Exp Hematol* 2004; 32: 1129–36.
52 Huang X, Cho S, Spangrude GJ. Hematopoietic stem cells: generation and self-renewal. *Cell Death Differ* 2007; 14: 1851–9.
53 Lawrence HJ, Christensen J, Fong S *et al.* Loss of expression of the HOXA-9 homeobox gene impairs the proliferation and repopulating ability of hematopoietic stem cells. *Blood* 2005; 106: 3988–94.
54 Waskow C, Paul S, Haller C, Gassmann M, Rodewald HR. Viable c-Kit (W/W) mutants reveal pivotal role for c-kit in the maintenance of lymphopoiesis. *Immunity* 2002; 17: 277–88.
55 Kimura S, Roberts AW, Metcalf D, Alexander WS. Hematopoietic stem cell deficiencies in mice lacking c-Mpl, the receptor for thrombopoietin. *Proc Natl Acad Sci USA* 1998; 95: 1195–200.
56 Antonchuk J, Hyland CD, Hilton DJ, Alexander WS. Synergistic effects on erythropoiesis, thrombopoiesis, and stem cell competitiveness in mice deficient in thrombopoietin and steel factor receptors. *Blood* 2004; 104: 1306–13.
57 Huntly BJ, Shigematsu H, Deguchi K *et al.* MOZ–TIF2, but not BCR–ABL, confers properties of leukemic stem cells to committed murine hematopoietic progenitors. *Cancer Cell* 2004; 6: 587–96.
58 Kindle KB, Troke PJ, Collins HM *et al.* MOZ–TIF2 inhibits transcription by nuclear receptors and p53 by impairment of CBP function. *Mol Cell Biol* 2005; 25: 988–1002.
59 Eklund EA. The role of HOX genes in malignant myeloid disease. *Curr Opin Hematol* 2007; 14: 85–9.

JOURNAL OF VIROLOGY, July 2008, p. 6395–6408
0022-538X/08/$08.00+0 doi:10.1128/JVI.00043-08

Vol. 82, No. 13

RUNX1 Permits E4orf6-Directed Nuclear Localization of the Adenovirus E1B-55K Protein and Associates with Centers of Viral DNA and RNA Synthesis▽

Leslie J. Marshall,[1]† Amy C. Moore,[2]† Misao Ohki,[3] Issay Kitabayashi,[3] David Patterson,[4] and David A. Ornelles[1]*

Department of Microbiology and Immunology, Wake Forest University School of Medicine, Winston-Salem, North Carolina 27157[1]; Department of Biochemistry, Vanderbilt University School of Medicine, Nashville, Tennessee 37232[2]; Molecular Oncology Division, National Cancer Center Research Institute, 5-1-1 Tsukiji, Chuo-ku, Tokyo, 104-0045, Japan[3]; and Eleanor Roosevelt Institute, Department of Biological Sciences, University of Denver, 2101 E. Wesley Ave., Denver, Colorado 80208[4]

Received 7 January 2008/Accepted 9 April 2008

The localization of the adenovirus E1B-55K–E4orf6 protein complex is critical for its function. Prior studies demonstrated that E4orf6 directs the nuclear localization of E1B-55K in human cells and in rodent cells that contain part of human chromosome 21. We show here that the relevant activity on chromosome 21 maps to *RUNX1*. RUNX1 proteins are transcription factors that serve as scaffolds for the assembly of proteins that regulate transcription and RNA processing. After transfection, the RUNX1a, RUNX1b, and RUNX1-ΔN variants allowed E4orf6-directed E1B-55K nuclear localization. The failure of RUNX1c to allow nuclear colocalization was relieved by the deletion of amino-terminal residues of this protein. In the adenovirus-infected mouse cell, RUNX1 proteins were localized to discrete structures about the periphery of viral replication centers. These sites are enriched in viral RNA and RNA-processing factors. RUNX1b and RUNX1a proteins displaced E4orf6 from these sites. The association of E1B-55K at viral replication centers was enhanced by the RUNX1a and RUNX1b proteins, but only in the absence of E4orf6. In the presence of E4orf6, E1B-55K occurred in a perinuclear cytoplasmic body resembling the aggresome and was excluded from the nucleus of the infected mouse cell. We interpret these findings to mean that a dynamic relationship exists between the E4orf6, E1B-55K, and RUNX1 proteins. In cooperation with E4orf6, RUNX1 proteins are able to modulate the localization of E1B-55K and even remodel virus-specific structures that form at late times of infection. Subsequent studies will need to determine a functional consequence of the interaction between E4orf6, E1B-55K, and RUNX1.

Human adenoviruses express genes early in a productive infection to create an environment suited for viral DNA replication, late gene expression, and virus assembly. The early region 1B 55-kDa (E1B-55K) and early region 4 open reading frame 6 (E4orf6) proteins are two such viral products that neutralize cellular antiviral responses (82) and promote late viral gene expression (7, 20, 24, 83). The E1B-55K and E4orf6 proteins form a physical complex in the nucleus of infected cells at late times of infection. This complex has been implicated in regulating mRNA transport by promoting the export of late viral messages while preventing the export of cellular messages (reviewed in reference 20). In addition, the complex directs the proteasome-dependent degradation of p53 (77), MRE11 (78), and DNA ligase IV (4) by reconfiguring a cellular ubiquitin ligase composed of Cul5, Rbx1, and elongins B and C (30, 67). Notably, mutant viruses that fail to express the *E1B-55K* or *E4orf6* genes are restricted for replication. This is due in part to the inability to promote the efficient transport of late viral RNA, which leads to reduced late viral gene expression (24). Because mRNA transport in adenovirus-infected cells is dependent on the proteasomal degradation machinery, the regulation of cellular and viral gene expression appears to depend on the activity of the E1B-55K–E4orf6 protein complex as a viral ubiquitin ligase (14, 83). The localization of the E1B-55K and E4orf6 proteins at late times of infection suggests that this activity is found in the nucleus of the infected cell (25, 60).

The E1B-55K and E4orf6 proteins shuttle between the nucleus and cytoplasm (18, 41) and accumulate in the nucleus of infected cells. The E4orf6 protein is evenly distributed throughout the nucleoplasm and is excluded from nucleoli (16). E1B-55K exhibits a complex distribution throughout the nucleus and cytoplasm. Within the nucleus at late times of infection, E1B-55K is distributed throughout the nucleus, is found in small filamentous spicules, and is concentrated about the periphery of the viral replication centers (25, 40, 60). These centers, sometimes called viral factories, have long been recognized as sites of viral DNA replication (49) and late viral RNA synthesis (48). Interestingly, E1B-55K fails to associate with the viral replication centers in cells infected with mutant viruses unable to express the *E4orf6* gene (60). The phenotype of the *E4orf6* mutant virus is similar to that of the *E1B-55K* mutant virus. Cells infected with *E4orf6* mutant viruses export late viral messages to the cytoplasm poorly compared to that by wild-type virus-infected cells (29, 32, 71) and fail to degrade cellular proteins such as p53, MRE11, and DNA ligase IV (4,

* Corresponding author. Mailing address: Medical Center Blvd., Department of Microbiology and Immunology, Wake Forest University School of Medicine, Winston-Salem, NC 27157. Phone: (336) 716-9332. Fax: (336) 716-9928. E-mail: ornelles@wfubmc.edu.

† L.J.M. and A.C.M. contributed equally to this work.

▽ Published ahead of print on 16 April 2008.

68, 77, 78). The ability of the E4orf6 protein to direct the association of E1B-55K to viral replication centers in the nucleus may be a critical element in the function of the E1B-55K–E4orf6 protein complex (25, 60).

When expressed by transfection, E1B-55K is restricted to the cytoplasm (26, 57). The E4orf6 protein is able to direct the nuclear localization of E1B-55K in primate cells but not in most rodent cells (13, 26). Because heterokaryons of human cells and rodent cells enabled the E4orf6 protein to retain E1B-55K in the rodent cell nucleus, we proposed that a primate-specific activity or factor promotes an interaction between the E1B-55K and E4orf6 proteins (26). Further studies mapped this activity to the distal region of human chromosome 21 (13). We report here that this activity mapped to human chromosome 21 is *RUNX1*, a gene previously identified as *AML-1*.

The RUNX1 proteins are so named because of their similarity to the Runt protein of *Drosophila melanogaster*, which was the first member of this family of proteins to be described (34). The RUNX1 proteins bind DNA and also serve as molecular scaffolds to promote protein-protein interaction at appropriate sites within the nucleus (31, 34, 87). At least four RUNX1 proteins have been described: RUNX1a, RUNX1b, RUNX1c, and RUNX1ΔN. These proteins are translated from alternatively spliced transcripts derived from two promoters (22, 44, 54). RUNX1 proteins are closely related to RUNX2 and RUNX3 proteins by their shared genomic architecture and through highly similar sequences in the amino terminus, called the Runt domain. The Runt domain is responsible for DNA binding (34, 56). RUNX1 proteins form the heterodimeric transcription factor identified as core binding factor (CBF), also known as the polyoma enhancer binding protein 2 (PEBP2), when associated with core binding factor beta (CBFβ) (56). RUNX1 members are involved in both transcriptional activation and repression during hematopoietic differentiation (34, 75). Consistently with their dual nature as scaffold proteins and DNA-binding transcription factors, RUNX1 proteins have a complex and dynamic physical structure composed of activation, inhibition, and negative regulatory domains (34). Negative regulatory regions for DNA binding and heterodimerization are present at both the amino and carboxyl termini. Signals within the cell of an unidentified nature cause these regions to mask the Runt domain and prevent it from associating with CBFβ or DNA (33). The RUNX1 proteins interact with many proteins within the nucleus, some of which act as corepressors of transcription while others act as coactivators (62). Proteins such as TLE1 and mSin3A are corepressors that contribute to RUNX1-mediated repression (47). RUNX1-associated coactivators include Myb and ALY/REF, which activate the T-cell receptor alpha enhancer; C/EBP, which promotes the coactivation of the macrophage colony-stimulating factor receptor promoter; and p300/CBP, which promotes the transcription of many genes required for myeloid cell differentiation (12, 36, 45). Interestingly, ALY/REF is deposited on newly synthesized mRNA in a sequence-independent manner and promotes efficient mRNA transport from the nucleus (61, 90). Therefore, the RUNX1 proteins may indirectly regulate mRNA transport by recruiting proteins such as ALY/REF to appropriate sites in the nucleus.

In this study, we demonstrate that human RUNX1 variants a, b, and ΔN promote the *E4orf6*-directed nuclear localization of E1B-55K in mouse cells, suggesting that it is the nuclear scaffold nature and not the DNA-binding ability of the RUNX1 protein that affects the apparent interaction between the E1B-55K and E4orf6 proteins. In addition, both endogenous RUNX1 protein and the RUNX1b variant protein localize at the periphery of virus replication centers at late times in adenovirus infection. RUNX1 localization at the virus replication centers appears to disrupt the normal localization of E4orf6 at these sites. In the absence of E4orf6, the RUNX1 proteins are able to retain E1B-55K at the periphery of virus replication centers. Therefore, E4orf6 and RUNX1 differentially affect the localization of E1B-55K during infection. Strikingly, viral replication centers were less developed in the absence of E1B-55K. However, the RUNX1b protein appeared to compensate for the absence of E1B-55K with respect to the development of viral replication centers. Taken together, these results suggest that the RUNX1b protein significantly affects the architecture of the virus replication center by mislocalizing the E4orf6 protein, ultimately leading to the inefficient trafficking of E1B-55K to the cytoplasm. The disruption of E4orf6–E1B-55K interactions at sites of virus replication within the nucleus could lead to defects in the virus replication cycle.

MATERIALS AND METHODS

Cells, plasmids, and viruses. Cell culture media, cell culture supplements, and sera were obtained from Invitrogen Life Technologies (Gaithersburg, MD) or HyClone (Logan, UT). Jurkat cells and Raji cells were maintained in HYQ RPMI-1640 (HyClone) medium supplemented with 10% fetal bovine serum (FBS). SaOS-2 cells were maintained in McCoy's 5a medium supplemented with 15% FBS. Mouse A9 cells were maintained in DMEM supplemented with 10% FBS. Mouse A9-21 cells were maintained in DMEM supplemented with 10% FBS and 400 U of hygromycin B per ml (15). The GM11130 cell line (Coriell Institute, Camden, NJ) was maintained in DMEM supplemented with 0.1 mM sodium hypoxanthine, 0.4 μM aminopterin, 16 μM thymidine, and 10% FBS. The GM10063 cell line (Coriell Institute) was maintained in DMEM supplemented with 0.1 mM sodium hypoxanthine, 0.4 μM aminopterin, 16 μM thymidine, and 15% FBS. The Chinese hamster ovary (CHO) cell lines bearing portions of human chromosome 21 (21q+, MRC-2G, 6918, R2-10W, Raj-5, 643C-13, 72532x6, and E7b) were generated at the Eleanor Roosevelt Institute (Denver, CO) and were previously described (27). CHO cell lines were maintained in Ham's F12 medium supplemented with 10% FBS.

The plasmids encoding *E1B-55K* and *E4orf6* under the control of both the T7 promoter and cytomegalovirus (CMV) immediate-early enhancer and promoter were described previously (26). The plasmids encoding human *RUNX2*, human *RUNX3*, mouse *Runx*1 (previously described as *PEBP2αC*, *PEBP2αA*, and *PEBP2αB*$_1$, respectively), and human *RUNXΔN* under the control of the human EF-1α promoter were described previously (89). The plasmids encoding the influenza virus hemagglutinin (HA) epitope-tagged *RUNX1a* and *RUNX1b* under the control of the simian virus 40 immediate-early promoter were described previously (39). These plasmids also confer resistance to G418 by directing the expression of the Tn*5* aminoglycoside 3′-phosphotransferase. The plasmid encoding human *RUNX1c* under the control of the CMV enhancer/promoter was kindly provided by Scott Hiebert (Vanderbilt University, Nashville, TN) and was described previously (53). The plasmid encoding an amino-terminally deleted RUNX1c under the control of the CMV enhancer/promoter was created by Scott Hiebert and kindly provided by Gary Stein (University of Massachusetts Medical School, Worcester). This RUNX1c plasmid originally was designated AML1b (or RUNX1b) but now has been correctly identified as RUNX1c. Herring sperm DNA was used as the carrier DNA in transfection experiments.

The adenovirus type 5 strain *dl*309 served as the wild-type adenovirus used in these studies. This virus is deleted of part of the E3 region that has been shown to be dispensable for growth in tissue culture (37). The E1B-55K mutant virus *dl*1520 contains a large deletion of the *E1B-55K* gene and is unable to express small splice variants of the larger E1B-55K protein. This virus has been previously described (5). The E1B-55K mutant virus *dl*338 contains a smaller deletion

of the E1B-55K region and can direct the expression of E1B proteins that are not expressed by *dl*1520 (63). The *E4orf6/E4orf7* mutant virus *dl*356, which expresses the *E4orf6* gene but not the *E4orf6/E4orf7* fusion product, was described previously (29). The *E4orf6* mutant virus used for this study was *dl*355*, which includes the wild-type *E3* gene, and was described previously (32). Viruses were grown in 293 cells, and concentrated virus stock was prepared by sequential centrifugation through CsCl gradients as previously described (26).

Antibodies. Adenovirus-specific antibodies included the mouse monoclonal antibody Rsa#3 (50) for the E4orf6 protein used as undiluted hybridoma culture supernatant fluid, the rat monoclonal antibody 9C10 (EMD Calbiochem, San Diego, CA) for the E1B-55K protein used at 1 μg per ml, the mouse monoclonal antibody 2A6 (72) for the E1B-55K protein used as undiluted hybridoma culture supernatant fluid, and the mouse monoclonal antibody B6-8 (70) for the E2A-DNA-binding protein (E2A-DBP) used as a fivefold diluted hybridoma culture supernatant fluid. Rabbit polyclonal antibodies against RUNX1 (Sigma, St. Louis, MO), RUNX2 (Active Motif, Carlsbad, CA), and RUNX3 (Active Motif) were used at 1:500 dilutions. HA-tagged RUNX1 proteins were visualized with the high-affinity rat monoclonal antibody 3F10 (Roche Diagnostics, Indianapolis, IN), which was used at 200 ng per ml. The mouse monoclonal antibody RmcB (CRL-2379; ATCC, Manassas, VA) against the coxsackie and adenovirus receptor (CAR) was used for cell sorting as the undiluted hybridoma culture supernatant fluid. Ubiquitin-specific antibody (clone P4D1; Cell Signaling Technology, Danvers, MA) was used at a 1:1,000 dilution. Fluorescently labeled secondary antibodies, qualified for multiple labeling experiments, were used at 1 to 4 μg per ml. These antibodies included Alexa Fluor 488 conjugated to goat anti-mouse immunoglobulin G (IgG) (Molecular Probes/Invitrogen), Alexa Fluor 568 conjugated to goat anti-rat IgG (Molecular Probes/Invitrogen), and rhodamine red X-conjugated goat anti-rat IgG (Jackson ImmunoResearch, West Grove, PA).

Stable HA-RUNX1a and HA-RUNX1b mouse A9 cell lines. Mouse A9 cells expressing HA-tagged human *RUNX1a* and *RUNX1b* cDNAs were generated by transfection and clonal selection. Briefly, 10^6 mouse A9 cells were transfected with 3 μg of *HA-RUNX1a* or *HA-RUNX1b* plasmid with Lipofectamine plus (Invitrogen Life Technologies) according to the manufacturer's recommendation. Two days after transfection, growth medium was replaced with medium supplemented with 600 μg of G418 per ml. Once all nontransfected cells died, single-transfected cell clones were obtained by serial dilution. Uniform *HA-RUNX1* expression was confirmed by immunofluorescence, and the appropriate protein size was confirmed by immunoblotting. Two separate clones were maintained for each RUNX1 protein by propagation in G418-containing medium.

Stable mouse A9 cell lines expressing the hCAR gene. Mouse A9 cells, HA-RUNX1a A9 cells, and HA-RUNX1b A9 cells were transduced with the pLXSN-based retrovirus expressing a carboxyl-terminally truncated variant of the human CAR (hCAR) (59). The virus was generously provided by James DeGregori (University of Colorado, Denver) through Linda Gooding (Emory University, Atlanta, GA). Working stocks of the retrovirus were produced as previously described (51). Because the HA-RUNX1 cells were resistant to G418, the virally transduced cells were selected by two rounds of staining for hCAR followed by cell sorting. Briefly, transduced cells were harvested in enzyme-free cell dissociation buffer (Invitrogen) and stained with the hCAR antibody RmcB for 1 h on ice, followed by being stained with Alexa Fluor 488-conjugated goat anti-mouse Ig for 30 min on ice. Cells were sorted using a FACSAria cell-sorting instrument (BD Biosciences, San Jose, CA). Sorted cells were maintained in medium containing 50 μg of G418 per ml to prevent microbial contamination. An additional round of cell sorting based on extracellular hCAR was performed to enrich for hCAR-positive cells.

Indirect immunofluorescence. Indirect immunofluorescence with intact cells was conducted as previously described (13). Briefly, cells were fixed with 2% freshly prepared formaldehyde and then permeabilized with 0.2% Triton X-100 before indirect antibody labeling. Infected Jurkat, Raji, SaOS-2, and *RUNX1*-expressing mouse A9 cells were extracted prior to fixation as described previously (60). Extraction with Triton X-100 enhances the visualization of viral replication centers by removing the diffuse nuclear component of E2A-DBP while sparing the replication center-associated protein (60, 81). Briefly, cells were washed twice in ice-cold phosphate-buffered saline with 1.5 mM $MgCl_2$ and then extracted for 5 min on ice with CSK buffer [100 mM KCl, 10 mM piperazine-*N*,*N*′-bis(2-ethanesulfonic acid) (pH 6.8), 300 mM sucrose, 3 mM $MgCl_2$, 1 mM ethylene glycol tetraacetic acid, 1 mM phenylmethylsulfonyl fluoride] containing 0.5% Triton X-100. Cells then were fixed with 2% formaldehyde in CSK buffer lacking Triton X-100 for 20 min at room temperature, followed by indirect immunofluorescence with the appropriate antibodies. Samples were mounted with a glycerol- or polyvinyl alcohol-based mounting medium containing the DNA dye 4′,6-dianidino-2-phenylindole (DAPI) and were analyzed by epifluorescence microscopy using a Nikon TE300 inverted microscope fitted with filters appropriate for DAPI, Alexa Fluor 488, and Alexa Fluor 568 excitation. Images were acquired using a Retiga EX 1350 digital camera (QImaging Corp., Burnaby, British Columbia, Canada) with a ×60 magnification/1.4-numerical aperture or ×100 magnification/1.4-numerical aperture oil immersion objective. The relative brightness and contrast of the digital images within each figure were adjusted to the same extent based on exposures obtained from control samples stained with secondary antibody alone. Figures were assembled with the open-source image-processing software ImageJ (69) and Canvas 10 (ACD Systems, Miami, FL) using either a Macintosh or Dell microcomputer. Color is used in some micrographs in which the adenovirus protein is shown in green and the RUNX protein in magenta so that colocalization is seen as white.

Quantitative evaluation of E4orf6-mediated nuclear E1B-55K localization. For the quantitative measurements reported in Fig. 1 and 4, cells were infected with recombinant vaccinia virus vTF7.3 (21) to express the T7 RNA polymerase and were transfected with cDNA for *E1B-55K* and *E4orf6* under the control of the T7 promoter. At 12 to 15 h postinfection (hpi), cells were fixed with formaldehyde before double-label immunofluorescence was performed to visualize the E4orf6 and E1B-55K proteins using the monoclonal antibodies Rsa#3 and 9C10, respectively. Cells in which at least a portion of E1B-55K was coincident in the nucleus with the E4orf6 protein and in which E4orf6 was excluded from the nucleoli were scored as nuclear. Approximately 6 to 10 randomly selected fields that were distributed uniformly across the culture surface were photographed in order to evaluate at least 200 to 400 cells in each experiment. Results from two to six independent experiments were pooled, and the 95% confidence intervals were estimated using the exact binomial test.

E4orf6-mediated E1B-55K nuclear localization was measured after the transient expression of selected *RUNX1* constructs shown in Table 1 by first transfecting 5×10^4 cells with 0.1 μg of *RUNX* plasmid using Lipofectamine plus (Invitrogen Life Technologies). Approximately 30 h after transfection, *E1B-55K* and *E4orf6* plasmids were expressed using the recombinant vaccinia virus vTF7.3, and the localization of the E1B-55K protein was determined as described above.

Functional mapping of human chromosome 21. The *E1B-55K* cDNA alone or the *E1B-55K* and *E4orf6* cDNAs were expressed in rodent cell lines containing various fragments of human chromosome 21 using the recombinant vaccinia virus vTF7.3, and the localization of the proteins was determined by double-label immunofluorescence as described above. Cell lines for which the frequency of E1B-55K–E4orf6 nuclear colocalization was greater than that of the parental (mouse or hamster) cell line were scored as positive.

Quantitative evaluation of the relative intensity of E1B-55K staining in the nucleus. The macro facility of the open-source software ImageJ (69) was used to quantify the ratio of nuclear to cytoplasmic staining for E1B-55K. Code and additional details will be provided upon request. Briefly, the expression of the *E1B-55K* and *E4orf6* cDNAs were established with the recombinant vaccinia virus vTF7.3 as described above. The cells were processed for immunofluorescence, and the localization of E1B-55K was recorded. A corresponding high-contrast image of the DAPI-stained nucleus was recorded and used to generate a binary image of the nuclear border that then was superimposed on the image of E1B-55K protein localization. A transect line was placed across each cell to be analyzed. Additional pseudorandomly distributed transect lines were generated automatically. The fluorescent intensity across the transect lines was measured, and the borders of the cell and the nucleus were recorded on each line. The mean fluorescent intensity outside of the cell was measured to serve as the local background. This value was subtracted from the mean fluorescent intensity for the nucleus and the cytoplasm before determining the ratio of nuclear to cytoplasmic fluorescence. Approximately 10 to 20 arbitrarily selected cells were analyzed, with four transect lines for each cell in each experiment.

RESULTS

Expressed by transfection, the E1B-55K and E4orf6 proteins colocalize in the nuclei of mouse cells containing the *RUNX1* locus of human chromosome 21. Mouse A9 fibroblast cells containing a copy of human chromosome 21 (15) were infected with a recombinant vaccinia virus to express the bacteriophage T7 polymerase. The infected cells were transfected with cDNA for the adenovirus E1B-55K protein or both E1B-55K and E4orf6 proteins under the direction of a T7 promoter, and the localization of the E4orf6 and E1B-55K proteins was determined by indirect immunofluorescence. Representative cells that received only the *E1B-55K* cDNA show predomi-

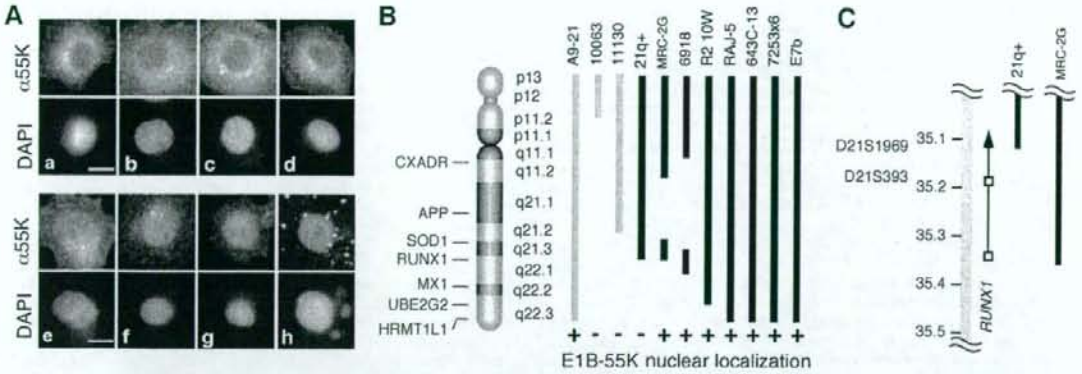

FIG. 1. E1B-55K and E4orf6 proteins colocalize in the nuclei of rodent cells containing the *RUNX1* locus of human chromosome 21. (A) Mouse A9 cells containing human chromosome 21 were infected with the recombinant vaccinia virus vTF7.3 to express the T7 RNA polymerase. The cells were transfected with cDNA for *E1B-55K* and *E4orf6* under the control of the T7 promoter. At 12 hpi, double-label immunofluorescence was used to identify cells expressing both *E4orf6* and *E1B-55K*. (A) Representative micrographs showing the localization of the E1B-55K protein, in which the localization was identified as predominantly cytoplasmic (a to d) or predominantly nuclear (e to h). The bar represents 5 μm. (B) Hamster (black) and mouse (gray) cells containing portions of human chromosome 21 were infected and transfected as described for panel A. At least three independent experiments were scored for the nuclear localization of E1B-55K. Cell lines that demonstrated the nuclear localization of E1B-55K in the presence of E4orf6 are indicated by a plus sign. (C) The portion of human chromosome 21 DNA in the 21q+ and MRC-2G hamster cells at the distal breakpoint is represented by black bars. Chromosome 21 is represented by the gray bar; the scale is indicate in megabase pairs. The approximate locations of STS markers are indicated. The *RUNX1* gene is represented by the arrow; open boxes identify the two *RUNX1* promoters.

nantly cytoplasmic staining for E1B-55K (Fig. 1A, images a to d). Cells transfected with cDNAs for both viral genes typically showed predominantly nuclear staining for E1B-55K (Fig. 1A, images e to h), although the relative intensity of nuclear staining varied among cells and not all cells contained predominantly nuclear E1B-55K protein. These results confirm previously reported findings (13) and illustrate the method used to score cells as containing predominantly nuclear E1B-55K protein.

Additional mouse and hamster cell lines containing portions of human chromosome 21 were evaluated as described above. At least three independent experiments were scored for the nuclear localization of E1B-55K. Cell lines that contained the nuclear localization of E1B-55K in the presence of the E4orf6 protein are indicated in Fig. 1B. E1B-55K remained cytoplasmic in all cell lines in the absence of the E4orf6 protein (data not shown). Both mouse (A9-21) and hamster (E7b, 72532x6, 643C-13, and Raj-5) cell lines with an intact copy of chromosome 21 as well as three hamster cell lines containing fragments of the chromosome (MRC-2G, 6918, and R2-10W) allowed the *E4orf6*-directed nuclear localization of E1B-55K (Fig. 1B).

TABLE 1. Human RUNX1 proteins permit E4orf6-directed nuclear localization of E1B-55K in mouse cells

Transfected construct	Cells with nuclear E1B-55K (%)	95% Confidence interval
Controls		
No E4orf6, no RUNX	1.3	0.36–4.8
No RUNX	6.2	3.0–1.3
Mouse Runx1		
Mouse Runx1b	3.5	0.5–25
Human RUNX related		
RUNX2 (6p21)	10.0	3.7–29
RUNX3 (1p36)	7.3	2.2–24
Human RUNX1		
RUNX1a	62.0	51–75
RUNX1b	63.0	36–100
RUNX1ΔN	50.0	49–52
RUNX1c	9.6	3.3–28
N terminus-deleted RUNX1c	50.0	49–52

The difference in the localization of E1B-55K between the 21q+ and MRC-2G cell lines was especially informative. By cytological criteria, the distal breakpoints of chromosome 21 in the MRC-2G and 21q+ cell lines appear identical. However, the 21q+ cell line, which does not permit E1B-55K protein nuclear localization, contains human chromosome 21 from the p terminus to sequence-tagged site (STS) marker D21S1969 and lacks STS marker D21S1950. By contrast, the distal fragment of chromosome 21 in the MRC-2G cell line, which permits E1B-55K protein nuclear localization, extends from the SOD1 marker to STS marker D21S393 (27). Therefore, this localizes the activity previously mapped to the q terminus of chromosome 21 that allows the *E4orf6*-directed nuclear localization of E1B-55K to a region of approximately 100 kb on chromosome 21. The only features identified in this region of chromosome 21 include *CLIC6*, a gene for an intracellular channel protein, and *RUNX1*, formerly known as *AML-1*. Because the RUNX1 proteins are nuclear proteins that mediate protein-protein interactions, we chose to investigate further the potential role of *RUNX1* in permitting *E4orf6*-directed nuclear localization.

A representation of the 260-kb *RUNX1* gene is shown in Fig. 2. The gene contains nine identified exons that are transcribed from telomere to centromere. *RUNX* genes express multiple

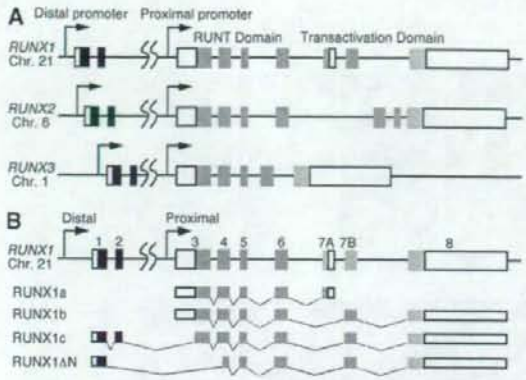

FIG. 2. Schematic representation of the human *RUNX1*, *RUNX2*, and *RUNX3* genes. (A) Boxes in the *RUNX* genes represent exons, open boxes represent noncoding exons, and shaded boxes indicate coding exons. The dual promoters, Runt domain, and transcriptional transactivation domains are highlighted. (B) The four major splice variants of *RUNX1* are indicated.

isoforms from two promoters. *RUNX1* encodes at least four isoforms in humans that arise from two promoters and alternative splicing (Fig. 2B). *RUNX1* transcripts originating from the proximal promoter are translated in a cap-independent manner under the direction of the large 5′-untranslated sequence that serves as an internal ribosome entry site (65). The distal *RUNX1* promoter directs the synthesis of mRNA translated by canonical cap-dependent means (65).

Human RUNX proteins accumulate at viral replication centers at late times during adenovirus infection. In human cells, the E4orf6 protein directs a portion of E1B-55K to the periphery of viral replication centers at late times of infection (60). These sites are thought to be a key site of E1B-55K–E4orf6 protein interaction within the nucleus (25, 40, 60). To determine if RUNX1 proteins also accumulate at viral replication centers, T-cell lymphoma-derived Jurkat cells, which contain abundant levels of RUNX1 proteins, were infected, and the localization of the endogenous RUNX1 protein was determined with respect to the E2A-DBP-stained replication centers. For comparison, the localization of the RUNX2 protein was determined in the osteosarcoma cell line SaOS-2, and the localization of the RUNX3 protein was determined in the Burkitt's B-cell lymphoma cell line Raji. In mock-infected cells, each RUNX protein exhibited a uniform granular staining pattern throughout the nucleus with exclusion from the nucleoli (Fig. 3a to f). The staining pattern for each RUNX protein changed after infection, such that a portion of the RUNX proteins relocalized to nuclear viral inclusions in the cells. Because these inclusions contained the E2A-DBP, we believe that these are sites of viral DNA replication and are the same as the viral replication centers that have been described previously for adenovirus-infected epithelial cells.

The localization of the RUNX protein with respect to the E2A-DBP differed among the different cell lines. The RUNX1 protein in the infected Jurkat cells was concentrated in discrete granules under 1 μm in diameter that formed a ring about the periphery of the E2A-DBP-containing structures (Fig. 3g and h). This localization resembled that of E1B-55K (see Fig. 2 of reference 60). A similar staining pattern was described by Bridge and associates for the snRNP proteins identified by the Y12 antibody in adenovirus-infected HeLa cells (11). These investigators suggested that this pattern was characteristic of cells at the onset of late transcription. By contrast, staining for both RUNX2 and RUNX3 was coincident with staining for the E2A-DBP, suggesting that the RUNX2 (Fig. 3i and j) and RUNX3 (Fig. 3k and l) proteins were found throughout the viral replication centers and perhaps were more closely associated with the viral DNA than with nascent viral RNA. Nonetheless, the superficially similar distribution of RUNX1, RUNX2, and RUNX3 in late-infected cells led us to test the possibility that the RUNX2 and RUNX3 proteins enhance the *E4orf6*-directed nuclear localization of E1B-55K in mouse cells.

A subset of RUNX1 proteins permits E4orf6-directed nuclear localization of E1B-55K in transfected mouse cells. Mouse A9 cells were transfected with cDNAs for each human *RUNX1* isoform or the predominant forms of human *RUNX2*, *RUNX3*, and mouse *Runx1*. The expression of the *E1B-55K* and *E4orf6* cDNAs was established, and the localization of E1B-55K in the presence of the E4orf6 protein was scored as cytoplasmic or nuclear as described for Fig. 1. Consistently with previous findings, whether expressed alone or coexpressed with *E4orf6* in mouse A9 cells, E1B-55K was restricted to the cytoplasm and perinuclear aggregates in over 90% of these cells (Table 1). The mouse Runx1b or human RUNX2 and RUNX3 proteins had no significant effect on the ability of *E4orf6* to direct nuclear E1B-55K protein localization. By contrast, RUNX1a, RUNX1b, and RUNX1ΔN proteins allowed *E4orf6*-directed nuclear E1B-55K protein localization in over 60% of the cells expressing the viral genes. Interestingly, RUNX1c was unable to promote E1B-55K nuclear localization. The RUNX1c protein contains a unique sequence in its amino-terminal portion (Fig. 2B) with the potential to prevent DNA binding and association with CBFβ (33). It is possible that this region, termed the negative regulatory region for heterodimerization and DNA binding, also prevents RUNX1c from affecting *E4orf6*-mediated E1B-55K protein nuclear localization. Evidence in support of this notion was derived from the property of an amino-terminally truncated RUNX1c variant that permitted E1B-55K nuclear localization. This variant contains an HA epitope tag in place of the first 26 amino acids of the RUNX1c amino terminus and therefore contains only 3 amino acids of the original RUNX1c negative regulatory region. This N-terminally deleted RUNX1c variant allowed the *E4orf6*-directed nuclear localization of E1B-55K in 50% of the mouse A9 cells (Table 1). This result suggests that sequences in the amino-terminal portion of RUNX1c can prevent RUNX1 from promoting *E4or6*-directed E1B-55K nuclear localization in mouse cells. These results also suggest that the ability to direct E1B-55K nuclear localization is not uniformly shared by RUNX1 variants. To overcome limitations associated with the transient expression required for these experiments, we established mouse A9 cell lines expressing *RUNX1a* and *RUNX1b* for further studies.

Expressed by transfection, the E1B-55K and E4orf6 proteins efficiently colocalize in the nuclei of mouse cells that express human *RUNX1a* and *RUNX1b*. Mouse A9 cells were

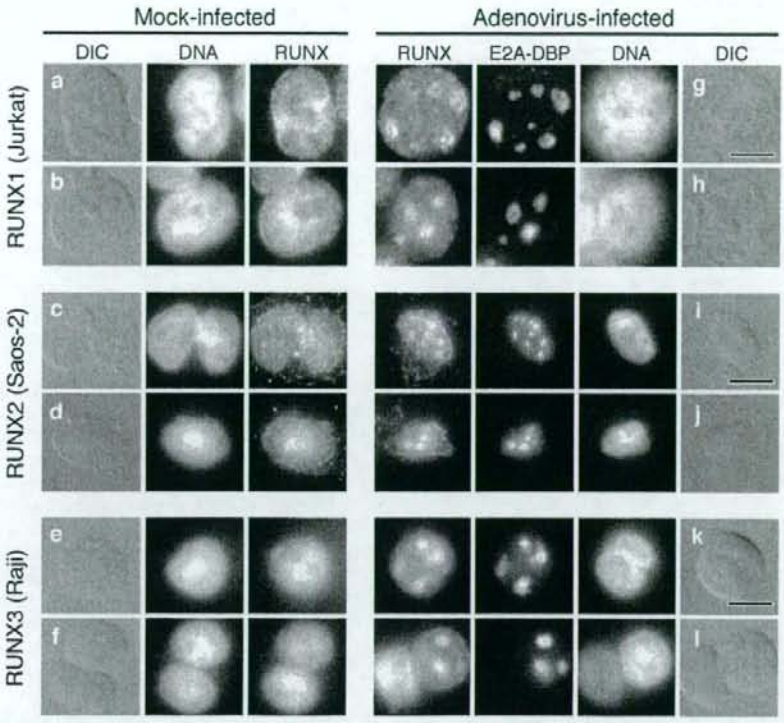

FIG. 3. Human RUNX proteins accumulate at viral replication centers at late times during adenovirus infection. Jurkat cells, SaOS-2 cells, and Raji cells were either mock infected (a to f) or infected with the wild-type virus *dl*309 (g to l). After 24 h, the cells were extracted with Triton X-100 as described in Materials and Methods. Viral replication centers were visualized with the mouse monoclonal antibody B6-8 against the E2A-DNA-binding protein, and the RUNX protein was simultaneously visualized with rabbit polyclonal antibodies specific for RUNX1 (a, b, g, and h), RUNX2 (c, d, i, and j), or RUNX3 (e, f, k, and l). DNA was visualized by being stained with DAPI. The bar in each differential interference contrast (DIC) image represents 10 μm.

transfected with plasmids encoding epitope-tagged human *RUNX1a* and *RUNX1b* cDNAs linked to a neomycin-selectable marker. Independent single-cell clones expressing *HA-RUNX1a* and *HA-RUNX1b* were isolated and designated HA-RUNX1a-A9 (clones 1 and 2) and HA-RUNX1b-A9 (clones 1 and 5). Uniform *RUNX1* expression was confirmed by immunofluorescence, and the predicted size of the protein was confirmed by immunoblotting (data not shown). It should be noted that repeated attempts to establish mouse cells expressing either epitope-tagged or native forms of *RUNX1c* and *RUNX1ΔN* using a variety of different expression constructs failed. The consistent failure to establish the expression of these two constructs leads us to suggest that mouse A9 cells cannot tolerate the stable expression of these particular forms of human *RUNX1* (data not shown). Curiously, the long-term expression of the *RUNX1b* construct also changed the growth properties of the A9 cells. The HA-RUNX1b cells grew more slowly and became difficult to detach from the culture vessel. The basis for these changes and their significance are not understood.

The nuclear localization assay for E1B-55K was performed as described for Fig. 1. As before, E1B-55K was restricted to the cytoplasm and perinuclear aggregates in the absence of the E4orf6 protein; this distribution was not affected by the RUNX1 protein. However, when coexpressed with *E4orf6*, E1B-55K was found in the nucleus of over 90% of the HA-RUNX1a-A9 and HA-RUNX1b-A9 cells (Fig. 4A). This result, which represents a substantial increase above the size of the fraction measured after transient transfection, confirms that both the RUNX1a and RUNX1b proteins permit the *E4orf6*-directed nuclear localization of E1B-55K.

Although both *RUNX1a* and *RUNX1b* enabled *E4orf6* to the direct the nuclear localization of E1B-55K in mouse cells, we observed differences in the staining intensity for the nuclear E1B-55K protein between the HA-RUNX1a and HA-RUNX1b cell lines. To determine if these differences were significant, the ratio of nuclear to cytoplasmic staining intensity for E1B-55K was quantified. This ratio was between 1 and 2 in the absence of E4orf6 (Fig. 4B). The coexpression of the *E4orf6* cDNA with the *E1B-55K* cDNA led to a substantial and statistically significant increase in the nuclear staining-to-cytoplasmic staining ratio in both the HA-RUNX1a and HA-RUNX1b A9 cell lines (Fig. 4B). No significant change in this ratio was measured for the vector-

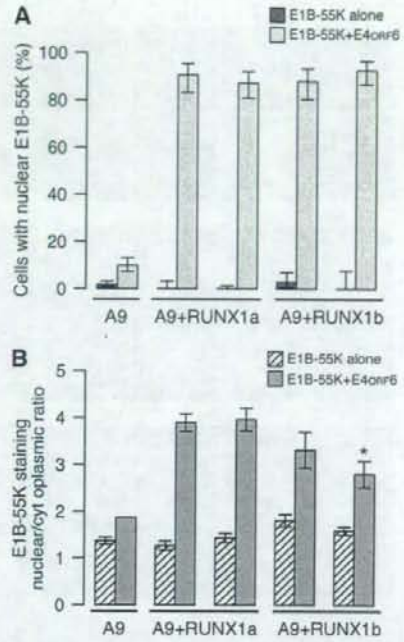

FIG. 4. E1B-55K and E4orf6 proteins efficiently colocalize in the nuclei of mouse cells that express human *RUNX1a* and *RUNX1b*. Two independent stable mouse A9 cell lines expressing human *RUNX1a* or *RUNX1b* were established, and the ability of *E4orf6* to direct the nuclear localization of E1B-55K was evaluated as described for Fig. 1. (A) Cells were scored as negative or positive for nuclear E1B-55K staining, and the percentages of cells with nuclear E1B-55K protein are indicated along with the standard errors of the means. (B) The ratio of nuclear to cytoplasmic staining for E1B-55K was quantified as described in Materials and Methods and is plotted as the means and standard deviations.

transfected A9 cell line (Fig. 4B and data not shown). However, both HA-RUNX1b cell lines showed greater cell-to-cell variability in the nuclear staining-to-cytoplasmic staining ratio. This difference was confirmed by an analysis of variance in which the variance for the HA-RUNX1b cells transfected with both E4orf6 and E1B-55K was 1.5-fold greater than that of RUNX1a cells ($P = 0.007$). The HA-RUNX1b cells also appeared to contain relatively less nuclear E1B-55K protein than the HA-RUNX1a cells. However, this decrease was statistically significant for only one of the two HA-RUNX1b-A9 cell lines (Fig. 4B) ($P < 0.002$ by Tukey's test for multiple comparisons). These results lead us to suggest that although *RUNX1a* and *RUNX1b* are able to permit the *E4orf6*-directed nuclear localization of E1B-55K, the RUNX1 isoforms are not identical in this regard.

RUNX1a and RUNX1b proteins differ in their association with viral replication centers in mouse cells. To determine if the RUNX1a and RUNX1b proteins associated with virus-specific structures in the infected mouse cell, the parental and HA-RUNX1 A9 mouse cell lines were transduced with a retrovirus to express the hCAR. After two rounds of enrichment for *CAR* expression, the cells were infected with adenovirus at an multiplicity of infection of ~1, corresponding to 300 to 1,000 viral particles. As noted by others, human adenovirus replicates more slowly in mouse cells than in human epithelial cells. Maximal early gene expression was observed at approximately 24 hpi, with peak virus production measured at 72 hpi (data not shown). Therefore, the infected cells were extracted with Triton X-100 at 24 hpi as described previously (60), and viral replication centers were visualized by staining for the E2A-DBP with a mouse monoclonal antibody. Extraction with Triton X-100 enhances the visualization of viral replication centers by removing the diffuse nuclear component of E2A-DBP while sparing the replication center-associated protein (81). The localization of the RUNX1 proteins was determined simultaneously using a rat monoclonal antibody for the HA epitope tag. Both RUNX1a and RUNX1b proteins exhibited a uniform granular staining pattern throughout the nucleus of mock-infected cells (data not shown). Both RUNX1a and RUNX1b proteins associated with the viral replication centers at late times of infection. However, the extent of this association differed, as seen in the representative cells shown in Fig. 5. In the majority of the cells, RUNX1a protein was observed at the periphery of the nuclear viral replication centers (Fig. 5c) or more coincident with E2A-DBP staining (data not shown). In the remaining infected cells, very little RUNX1a protein was associated with viral replication centers (Fig. 5d). In all infected HA-RUNX1a cells, a significant portion of the RUNX1a protein remained diffusely distributed throughout the nucleus. By contrast, over 90% of the HA-RUNX1b cells contain distinct viral replication centers surrounded by staining for the RUNX1b protein. The RUNX1b protein was not coincident with E2A-DBP. Rather, the RUNX1b protein was primarily at the periphery of the replication centers (Fig. 5f). These results demonstrate that the RUNX1a and RUNX1b proteins associate with centers of viral DNA replication in the infected mouse cell but that the nature of this association differs between the two proteins.

RUNX1 displaces E4orf6 from viral replication centers in adenovirus-infected mouse cells. A portion of the E4orf6 protein localizes to the periphery of viral replication centers in HeLa cells (60). To determine if the E4orf6 protein showed a similar localization in mouse cells, A9-hCAR and HA-RUNX1 A9 cells were infected and stained for the E4orf6 and HA-tagged RUNX1 proteins. For these experiments, the RUNX1 protein was used as a marker for viral replication centers, because both E2A-DBP and E4orf6 antibodies are mouse antibodies, precluding their use for double labeling. At 24 hpi, approximately 25% of the infected parental A9-hCAR cells displayed a strong E4orf6-specific staining pattern resembling that of viral replication centers (Fig. 6a and b). This distribution and its frequency were similar to those observed in infected human cells. Remarkably, the E4orf6 protein was no longer concentrated about the viral replication centers in A9 cells expressing *RUNX1a* or *RUNX1b*. Although viral replication centers were readily visualized by staining for the appropriate RUNX1 protein, the E4orf6 protein was uniformly distributed through the nucleus and was excluded from nucleoli (Fig. 6c, e, and f). In a representative experiment, only 13 of 75 (17%) HA-RUNX1a cells with distinct viral replication centers showed any indication of increased E4orf6 staining at these

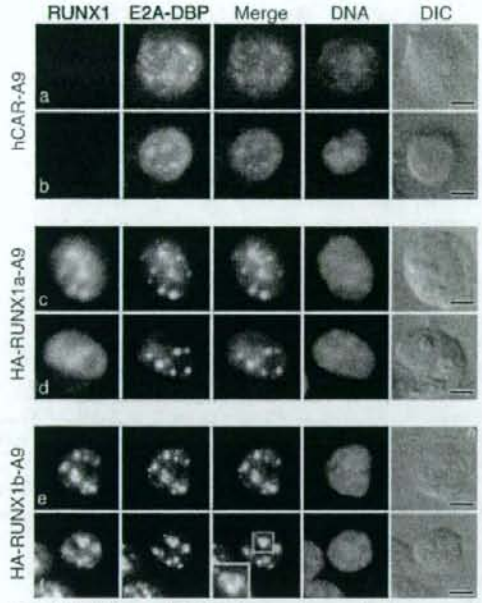

FIG. 5. RUNX1a and RUNX1b proteins vary in the extent of association with viral replication centers. Mouse A9 cells that express *hCAR* were transduced with vector DNA (a and b) or cDNA of HA-tagged human *RUNX1a* (c and d) or HA-tagged human *RUNX1b* (e and f) and were infected with the wild-type virus *dl*309. After 24 h, the cells were extracted with Triton X-100 as described in Materials and Methods, and double-label immunofluorescence was performed to visualize viral replication centers with the monoclonal antibody B6-8 against the E2A-DBP and a rat monoclonal antibody against the HA epitope. In the merged image, E2A-DBP is shown in green and RUNX1 is shown in magenta. (f) The inset in the merge image shows RUNX1 protein (magenta) surrounding the E2A-DBP (green). DNA was visualized by being stained with DAPI and is shown in blue. Representative micrographs are shown; the bar in each differential interference contrast (DIC) image represents 5 μm.

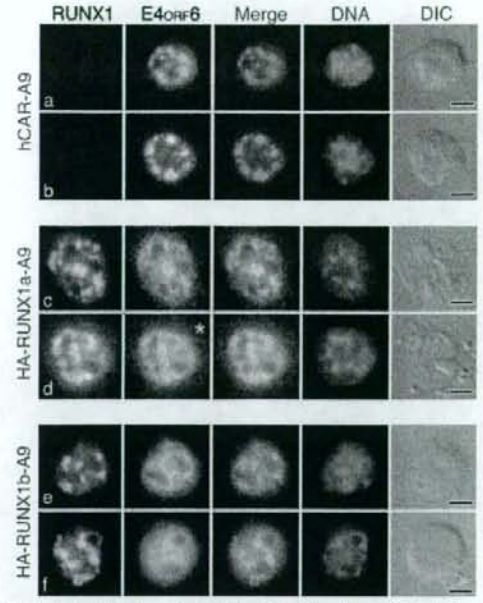

FIG. 6. RUNX1b precludes E4orf6 localization at the periphery of viral replication centers. The *hCAR*-transduced mouse A9 cells analyzed in Fig. 5 were infected with the *E4orf6/E4orf7* mutant virus *dl*356. After 24 h, the cells were extracted with Triton X-100 as described in Materials and Methods and processed for double-label immunofluorescence using the E4orf6-specific antibody Rsa#3 and the HA-specific rat antibody. The phenotypically wild-type virus *dl*356 was used for this experiment, because the Rsa#3 antibody recognizes both E4orf6 protein and the 17-kDa E4orf6/E4orf7 fusion protein. In the absence of staining for the E2A-DBP, viral replication centers can be recognized by differential interference contrast (DIC) illumination or by the absence of DAPI staining in the DNA image. In the merged image, the E4orf6 protein is shown in green and RUNX1 is shown in magenta. DNA was visualized by being stained with DAPI and is shown in blue. Representative micrographs are shown, except for that for the HA-RUNX1a cell in panel d. This cell represents a rare cell displaying (<5%) E4orf6 protein concentrated about the viral replication centers defined by RUNX1 staining. The bar in each DIC image represents 5 μm.

centers. Furthermore, the intensity of E4orf6 staining at the replication centers in these few cells was substantially less than that observed in A9-hCAR cells (compare Fig. 6b to Fig. 6d). In the same experiment, none of 85 HA-RUNX1b cells with distinct replication centers showed increased E4orf6 staining at these centers (Fig. 6e and f). These results indicate that the RUNX1 proteins displace or preclude E4orf6 from concentrating at the viral replication centers in the infected mouse cell, with the RUNX1b protein showing a stronger ability to perturb E4orf6 localization at the viral replication centers compared to that of the RUNX1a protein.

E4orf6 and RUNX1 exert different effects on the localization of E1B-55K in adenovirus-infected mouse cells. In contrast to the ability of the RUNX1 proteins to perturb E4orf6 protein localization, the RUNX1 proteins had no apparent impact on the localization of E1B-55K in mouse cells infected with the wild-type virus. In these cells, E1B-55K occurred primarily in a perinuclear cytoplasmic inclusion body (Fig. 7). Virtually identical staining patterns for E1B-55K were observed for A9-hCAR, HA-RUNX1a, and HA-RUNX1b A9 cells. Similar perinuclear inclusions of E1B-55K were observed in adenovirus-transformed rodent cells (86). Recently, inclusion bodies similar in appearance to these were identified as aggresomes and are associated with the terminal stages of E1B-55K–E4orf6-mediated protein degradation (1, 46). An antibody to ubiquitin revealed pronounced staining of cytoplasmic bodies of the same frequency and relative position to the nucleus as the perinuclear E1B-55K bodies in the infected mouse cells. This observation is consistent with the possibility that this structure is an aggresome (data not shown). These results distinctly differ from findings from human cells in which a portion of the E1B-55K and E4orf6 proteins colocalized at the periphery of viral replication centers. Therefore, although the RUNX1 proteins promote the nuclear colocalization of the E4orf6 and E1B-55K proteins after transfection, the RUNX1 proteins fail to exert a similar influence following infection.

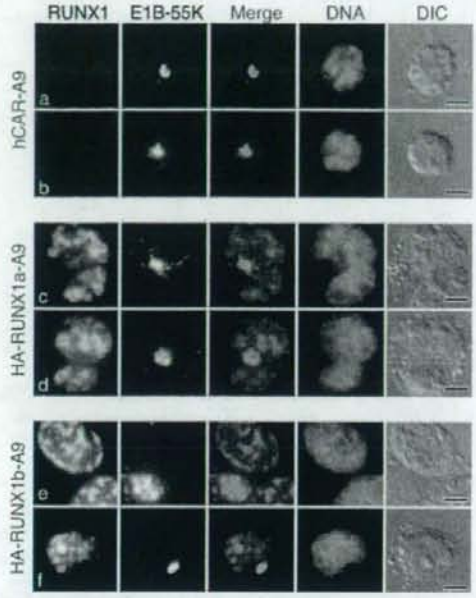

FIG. 7. E1B-55K accumulates at cytoplasmic structures resembling the aggresome in wild-type virus-infected mouse A9 cells. The *hCAR*-transduced mouse A9 cells analyzed in Fig. 5 were infected with the wild-type virus *dl*309. After 24 h, the cells were extracted with Triton X-100 as described in Materials and Methods and processed for double-label immunofluorescence using the E1B-55K-specific mouse monoclonal antibody 2A6 and the HA-specific rat antibody. In the merged image, E1B-55K is shown in green and RUNX1 is shown in magenta. DNA was visualized by being stained with DAPI and is shown in blue. The bar represents 5 μm. DIC, differential interference contrast.

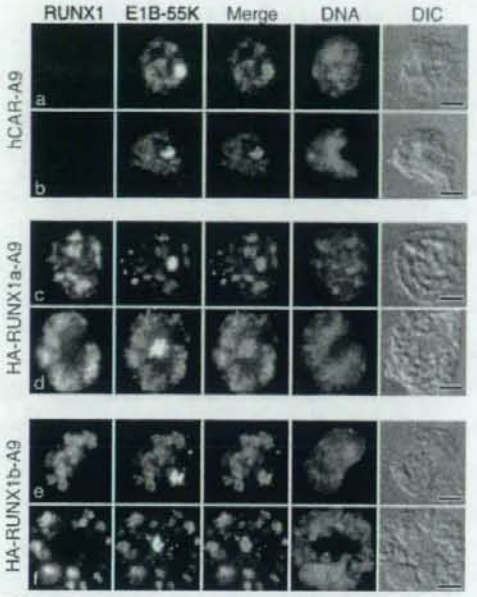

FIG. 8. E4orf6 and RUNX1 differentially affect the localization of E1B-55K in adenovirus-infected mouse cells. The *hCAR*-transduced mouse A9 cells analyzed in Fig. 5 were infected with the *E4orf6* mutant virus *dl*355*. After 24 h, the cells were extracted with Triton X-100 as described in Materials and Methods and processed for double-label immunofluorescence after 24 h using the E1B-55K-specific mouse monoclonal antibody 2A6 and the HA-specific rat antibody. In the merged image, E1B-55K is shown in green and RUNX1 is shown in magenta. DNA was visualized by being stained with DAPI and is shown in blue. The bar represents 5 μm. DIC, differential interference contrast.

To determine if the E4orf6 protein had any impact on E1B-55K localization in the infected mouse cell, cells were infected with the *E4orf6* mutant virus *dl*355* and E1B-55K was visualized. As in wild-type virus-infected cells, some of the E1B-55K protein accumulated in the aggresome. Surprisingly, a significant portion of E1B-55K remained in the infected hCAR-A9 mouse cell nucleus in the absence of the E4orf6 protein (Fig. 8a and b). Furthermore, some cells displayed a limited association between E1B-55K and viral replication centers (Fig. 8a). The localization of E1B-55K at the periphery of virus replication centers increased in both HA-RUNX1a (Fig. 8c and d) and HA-RUNX1b (Fig. 8e and f) cells. In HA-RUNX1b cells with prominent viral replication centers, most of the nuclear E1B-55K protein was coincident with staining for the RUNX1b protein. Taken together with the results shown in Fig. 7, these findings indicate that *E4orf6* acts in a dominant manner to exclude E1B-55K from the nucleus of infected mouse cells. In the absence of *E4orf6*, the RUNX1a and RUNX1b proteins promote the retention of E1B-55K at viral replication centers. Furthermore, the similarity of HA-RUNX1 staining in cells infected with the wild-type virus (Fig. 7) and E4orf6 mutant virus (Fig. 8) reveals that *E4orf6* has little impact on the localization of the RUNX1 proteins.

E1B-55K promotes the formation of viral replication centers, and RUNX1b can compensate for the loss of E1B-55K. Cells were infected with the *E1B-55K* mutant virus *dl*1520 in order to determine if E1B-55K affected the localization of the RUNX1 proteins. The infected cells were extracted with Triton X-100 after 24 h, and the RUNX1 protein and E2A-DBP were visualized by double-label immunofluorescence as before. Surprisingly, no E2A-DBP staining was evident in the Triton X-100-extracted HA-RUNX1a cells. However, nonextracted cells were uniformly stained for E2A-DBP throughout the nucleus. Identical results were obtained following infection with the E1B mutant virus *dl*338 (63), which also bears a deletion in the E1B-55K coding region but is able to direct the expression of minor E1B-55K-related proteins that are not expressed by *dl*1520 (data not shown). Thus, the failure to see staining in the extracted cells was due to the unexpected discovery that E1B-55K is required for well-developed viral replication centers to form in hCAR-A9 and HA-RUNX1a A9 cells (Fig. 9a to d). In HA-RUNX1a cells infected with the *E1B-55K* mutant virus, the RUNX1a protein was diffusely distributed throughout the nucleus and excluded from the nucleoli (Fig. 9c and d). These results show that the absence of E1B-55K affects the localization of RUNX1a, which fails to

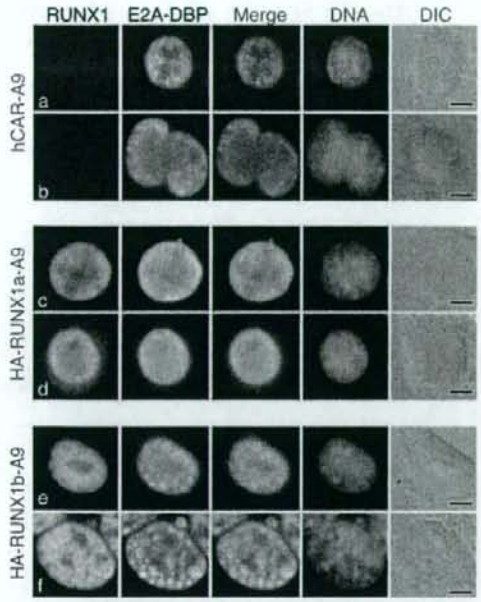

FIG. 9. E1B-55K supports the formation of virus replication centers, and RUNX1b can compensate for the loss of E1B-55K in adenovirus-infected mouse cells. The *hCAR*-transduced mouse A9 cells analyzed in Fig. 5 were infected with the *E1B-55K* mutant virus *dl*1520 and processed for double-label immunofluorescence as intact cells after 24 h using the E2A-DBP-specific mouse monoclonal antibody B6-8 and the HA-specific rat antibody. In the merged image, E2A-DBP is shown in green and RUNX1 is shown in magenta. DNA was visualized by being stained with DAPI and is shown in blue. The bar represents 5 μm. DIC, differential interference contrast.

accumulate at viral replication centers. However, it seems likely that this is a secondary effect due to the failure to form viral replication centers in the mutant virus-infected RUNX1a-expressing cells.

In sharp contrast to *dl*1520-infected HA-RUNX1a cells, viral replication centers were prominent and abundant in HA-RUNX1b cells that were infected with the *E1B-55K* mutant virus. The staining pattern for E2A-DBP in the mutant virus-infected HA-RUNX1b cells (Fig. 9e and f) was similar to that of wild-type virus-infected cells (Fig. 5e and f). Again, the RUNX1b protein was found at the periphery of the viral replication centers, often forming concentric rings about the E2A-DBP-containing structures (Fig. 9f). These results indicate that in mouse A9 cells, E1B-55K is necessary for the efficient development of viral replication centers. Furthermore, these results reveal a striking functional difference between the RUNX1a and RUNX1b proteins, wherein only RUNX1b can compensate for the absence of *E1B-55K* expression by promoting the development of viral replication centers.

DISCUSSION

In this study, we identify the previously described activity on human chromosome 21 (13) that allows *E4orf6* to direct the nuclear localization of E1B-55K following transfection in rodent cells. This activity maps to the *RUNX1* gene at 21q22.3. The human RUNX1 protein variants a, b, and ΔN, but not RUNX1c, permit the *E4orf6*-directed nuclear localization of E1B-55K. Human *RUNX1b* and *RUNX1c* mRNAs were detected by reverse transcription followed by PCR, and RUNX1-related proteins of the appropriate size were detected by immunoblotting the A9-21 mouse cell line that carries human chromosome 21 (data not shown). Because we show here that the RUNX1a, RUNX1b, and RUNX1ΔN variants, but not the RUNX1c variant, permit *E4orf6*-directed E1B-55K nuclear localization in mouse cells, we suggest that the relevant activity detected in the A9-21 cells was that of RUNX1b.

RUNX1 proteins are canonical DNA-binding transcription factors that serve as a scaffold for the assembly of a multiprotein complex. This complex can include both transcriptional coactivators and corepressors (62). The RUNX1 isoforms differ in their ability to bind DNA and transcriptional modulators (34). We show here that three of the four major RUNX1 variants (a, b, and ΔN) permitted the *E4orf6*-directed nuclear localization of E1B-55K in mouse cells. It seems reasonable that this property resides in the sequence common to these three proteins, which is limited to part of the Runt domain encoded by exons 4, 5, and 6. However, this sequence is not sufficient for this activity, because RUNX1c, which also contains this sequence, does not permit E1B-55K nuclear localization. RUNX1c contains 31 more amino-terminal residues than RUNX1b. This domain can interfere with binding to both DNA and the heterodimerization partner CBFβ (33). The results reported here indicate that the negative regulatory amino-terminal domain also precludes RUNX1c from promoting the *E4orf6*-mediated nuclear localization of E1B-55K. Further support for this idea derives from a mutant form of RUNX1c in which all but three amino acids of the unique N terminus were replaced with an epitope tag. This variant permitted the *E4orf6*-directed nuclear localization of E1B-55K as effectively as the RUNX1a and RUNX1b proteins. RUNX1ΔN is missing 12 of the 31 amino acids in the amino terminus and half of the DNA-binding Runt domain. This variant is unable to bind DNA (88). However, RUNX1ΔN allowed *E4orf6*-directed E1B-55K nuclear localization, indicating that the ability to bind DNA is dispensable for the RUNX1 proteins to affect E1B-55K–E4orf6 colocalization. These results lead us to suggest that the scaffolding nature of the RUNX1 proteins is important for their ability to affect the *E4orf6*-directed nuclear localization of E1B-55K.

In contrast to the relatively simple relationship between E1B-55K, E4orf6, and the RUNX1 proteins observed in transfected cells, the behavior of these proteins in adenovirus-infected cells is complex. Endogenous RUNX1 protein present in Jurkat cells and human RUNX1a and RUNX1b proteins expressed in mouse cells accumulate about the periphery of viral replication centers at late times of infection. This localization, which is close to sites of late viral RNA biogenesis, does not depend on either *E1B-55K* or *E4orf6*. Also, because viral DNA replication proceeded with similar kinetics among RUNX1-expressing cell lines (data not shown), it seems unlikely that different rates of viral DNA synthesis affected protein localization about viral replication centers. Rather, the RUNX1 proteins appear to expel most of the E4orf6 protein

from these sites. Furthermore, instead of retaining E1B-55K in the nucleus of adenovirus-infected mouse cells, *E4orf6* expression excludes E1B-55K from the nucleus of infected mouse cells. In the absence of *E4orf6* expression, E1B-55K accumulates in the nucleus and at viral replication centers; this localization is enhanced by the RUNX1b protein. Although RUNX1 may increase the retention of E1B-55K at viral replication centers by expelling a portion of E4orf6 from these sites, we predict that RUNX1 disrupts functions of the E1B-55K–E4orf6 protein complex. Because E1B-55K rapidly shuttles between the nucleus and cytoplasm of transfected (41) and infected cells (18), we interpret these findings to suggest that the E4orf6 protein accelerates the trafficking of E1B-55K through the nucleus, which ultimately results in its accumulation in structures resembling the aggresome in the infected mouse cell. Recently, the trafficking of the E1B-55K protein from the nucleus to the aggresome has been linked to the sequestration of the candidate tumor suppressor protein, sequence-specific single-stranded DNA-binding protein 2 (19).

The E1B-55K protein is a multifunctional protein with a complex distribution throughout the nucleus and cytoplasm of the adenovirus-infected cell. The intracellular trafficking of E1B-55K is affected by interactions with viral factors such as the E4orf3 (42, 43) and E4orf6 proteins (17, 58, 60) as well as cellular factors such as elongins B and C, Cullin5, and RING Box protein-1 (30, 67). With some of these binding partners, the E1B-55K and E4orf6 proteins form a virus-specific E3 ubiquitin ligase that, among other activities, regulates mRNA transport (see especially references 7, 20, and 83). A portion of the E1B-55K protein localizes to nodules or crenulations about the periphery of viral replication centers; this localization is reduced during infection with *E4orf6* mutant viruses (60). These nodules and crenulations are enriched in splicing factors and viral RNA (9, 11, 64) and are the initial sites of late viral transcription and RNA processing (2, 3, 64). The localization of RUNX1 to these sites is consistent with the possibility that the RUNX1 proteins alter viral RNA biogenesis through the E1B-55K–E4orf6 protein complex. In the infected mouse cells, RUNX1b is found at the viral replication centers at a much higher frequency than RUNX1a. Staining for RUNX1b at the periphery of these structures resembles staining for small nuclear ribonucleoproteins in ring cells described by Aspegren and Bridge (2, 3). Because the localization of RUNX1b at these sites expels some of the E4orf6 protein, RUNX1b may disrupt the function of the E1B-55K–E4orf6 protein complex. We previously reported that a greater fraction of rodent cells with the q terminus of human chromosome 21 expressed late viral genes than cells without that fragment of human DNA (13). However, a comparable effect on virus yield was not observed in these studies. Consequently, the results reported here will guide additional studies to elucidate the impact of specific RUNX1 variants on adenovirus replication.

Centers of viral DNA replication and late viral transcription, termed viral factories, viral inclusion bodies, viral centers, or viral replication centers, are complex structures that evolve during the course of a virus infection (see, for example, references 3, 6, 10, and 66). Specific localizations within this structure during the late phase of an infection can indicate function. The RUNX1b protein is found in the peripheral replicative zone (66), which has been shown to be the site of late viral RNA processing. Staining for the RUNX1 protein in the T-cell lymphoma Jurkat cell line most closely resembled staining for the RUNX1b protein. By contrast, RUNX1a was most often coincident with the E2A-DBP, which is linked to accumulations of single-stranded viral DNA in the virus replication centers. These E2A-DBP-rich sites are devoid of factors involved in RNA processing (64). This localization was most similar to that of the RUNX2 and RUNX3 proteins in SaOS-2 and Raji cells, respectively. It is possible that common properties of the RUNX proteins, such as the Runt DNA-binding domain, enable the RUNX proteins to associate with the viral replication centers while specific protein-protein interactions target this protein to substructures at these sites. The molecular basis for the association between the RUNX1 proteins and the adenovirus proteins as well as virus-specific structures in the infected cell remains to be elucidated.

The RUNX1 proteins are important regulators of transcription and replication for several viruses. As the DNA-binding component of the core binding factor, the larger RUNX1 proteins regulate transcription from viral enhancers in murine leukemia viruses (73, 84, 85), maedi visna virus (79), and polyomavirus (reviewed in reference 76). It has been suggested that RUNX1 proteins contribute to the E2-mediated repression of bovine and human papillomavirus transcription (8, 74). Mouse Runx1 was identified as a protein that binds polyomavirus DNA and activates viral DNA replication (38). The inability of polyomavirus to replicate in mouse embryonal carcinoma cells has been attributed to the absence of the Runx1 protein (35). Recently, Runx1 was shown to be recruited to virus replication factories during polyomavirus infection. At these sites, Runx1 was proposed to couple the viral DNA to the nuclear matrix while recruiting T antigen to the origin of replication (55). Although the contribution of RUNX1 to the outcome of an adenovirus infection has yet to be determined, the findings we report here suggest that the DNA-binding ability of RUNX1 is not important for adenovirus. Rather, because of the similar distribution for RUNX1b and viral RNA and RNA processing factors, we suggest that properties of RUNX1 that link it to RNA processing, such as the ability to bind ALY/REF (12), will be important to the outcome of an adenovirus infection.

In summary, the results presented here reveal a dynamic relationship between the E4orf6, E1B-55K, and RUNX1 proteins. In cooperation with the E4orf6 protein, RUNX1 proteins are able to affect the localization of E1B-55K. The localization of RUNX1b in the infected cell is consistent with a possible role for this cellular protein in modulating viral RNA metabolism. Additional studies are required to determine the molecular mechanism by which these proteins interact or influence the localization of each other. It also will be important to determine if the activity of the E1B-55K–E4orf6 protein complex is altered in human cells with high levels of the RUNX1 proteins. Lymphocytic cells express high levels of *RUNX1* at various stages in development. Interestingly, some of these cells are able to harbor adenovirus in a quiescent or possibly latent state (23, 52). Perhaps by targeting the E1B-55K–E4orf6 protein complex, the RUNX1 proteins can suppress adenovirus gene expression as part of a program to establish the quiescent state. We show here that RUNX1a and RUNX1b exert significant differences on the development of virus-specific structures in the infected cell. Recently, human

RUNX1a and *RUNX1b* were shown to differ in their ability to promote hematopoietic stem cell expansion and differentiation (80). In human cord blood lymphocytes, *RUNX1a* expression was restricted to the $CD34^+$ progenitor cells and was highest in the most primitive $CD34^+$ compartment (80). The recently identified association between adenovirus and childhood acute lymphocytic leukemia (28) makes it important to evaluate the impact of RUNX1 expression on the outcome of an adenovirus infection in the developing hematopoietic compartment.

ACKNOWLEDGMENTS

We thank Scott Hiebert (Vanderbilt University) and Gary Stein (University of Massachusetts, Worcester) for generously providing RUNX1 plasmids, Tom Shenk (Princeton University), Arnie Berk (UCLA), and Pat Hearing (SUNY Stony Brook) for mutant adenoviruses, and James DeGregori for the hCAR retrovirus. We especially thank Isabelle Berquin, Nathan Iyer, and James Woods (WFU Health Sciences) for their help in creating hCAR-transduced cells. We thank Linda Gooding (Emory University) for valuable discussions during this work.

Cell culture reagents and services were provided by the Cell and Virus Vector Core Laboratory, a service of the Comprehensive Cancer Center of Wake Forest University, which is supported in part by the National Cancer Institute grant CA 12197. This work was supported by the Towne Foundation (D.P.) and Public Health Service grant CA 77342 from the National Cancer Institute to D.A.O.

REFERENCES

1. **Araujo, F. D., T. H. Stracker, C. T. Carson, D. V. Lee, and M. D. Weitzman.** 2005. Adenovirus type 5 E4orf3 protein targets the Mre11 complex to cytoplasmic aggresomes. J. Virol. **79:**11382–11391.
2. **Aspegren, A., and E. Bridge.** 2002. Release of snRNP and RNA from transcription sites in adenovirus-infected cells. Exp. Cell Res. **276:**273–283.
3. **Aspegren, A., C. Rabino, and E. Bridge.** 1998. Organization of splicing factors in adenovirus-infected cells reflects changes in gene expression during the early to late phase transition. Exp. Cell Res. **245:**203–213.
4. **Baker, A., K. J. Rohleder, L. A. Hanakahi, and G. Ketner.** 2007. Adenovirus E4 34k and E1b 55k oncoproteins target host DNA ligase IV for proteasomal degradation. J. Virol. **81:**7034–7040.
5. **Barker, D. D., and A. J. Berk.** 1987. Adenovirus proteins from both E1B reading frames are required for transformation of rodent cells by viral infection and DNA transfection. Virology **156:**107–121.
6. **Besse, S., and F. Puvion-Dutilleul.** 1994. Compartmentalization of cellular and viral DNAs in adenovirus type 5 infection as revealed by ultrastructural in situ hybridization. Chromosome Res. **2:**123–135.
7. **Blanchette, P., C. Y. Cheng, Q. Yan, G. Ketner, D. A. Ornelles, T. Dobner, R. C. Conaway, J. W. Conaway, and P. E. Branton.** 2004. Both BC-box motifs of adenovirus protein E4orf6 are required to efficiently assemble an E3 ligase complex that degrades p53. Mol. Cell. Biol. **24:**9619–9629.
8. **Boeckle, S., H. Pfister, and G. Steger.** 2002. A new cellular factor recognizes E2 binding sites of papillomaviruses which mediate transcriptional repression by E2. Virology **293:**103–117.
9. **Bridge, E., M. Carmo-Fonseca, A. Lamond, and U. Pettersson.** 1993. Nuclear organization of splicing small nuclear ribonucleoproteins in adenovirus-infected cells. J. Virol. **67:**5792–5802.
10. **Bridge, E., and U. Pettersson.** 1996. Nuclear organization of adenovirus RNA biogenesis. Exp. Cell Res. **229:**233–239.
11. **Bridge, E., D. X. Xia, M. Carmo-Fonseca, B. Cardinali, A. I. Lamond, and U. Pettersson.** 1995. Dynamic organization of splicing factors in adenovirus-infected cells. J. Virol. **69:**281–290.
12. **Bruhn, L., A. Munnerlyn, and R. Grosschedl.** 1997. ALY, a context-dependent coactivator of LEF-1 and AML-1, is required for TCRα enhancer function. Genes Dev. **11:**640–653.
13. **Chastain-Moore, A. M., T. Roberts, D. A. Trott, R. F. Newbold, and D. A. Ornelles.** 2003. An activity associated with human chromosome 21 permits nuclear colocalization of the adenovirus E1B-55K and E4orf6 proteins and promotes viral late gene expression. J. Virol. **77:**8087–8098.
14. **Corbin-Lickfett, K. A., and E. Bridge.** 2003. Adenovirus E4-34kDa requires active proteasomes to promote late gene expression. Virology **315:**234–244.
15. **Cuthbert, A. P., D. A. Trott, R. M. Ekong, S. Jezzard, N. L. England, M. Themis, C. M. Todd, and R. F. Newbold.** 1995. Construction and characterization of a highly stable human: rodent monochromosomal hybrid panel for genetic complementation and genome mapping studies. Cytogenet. Cell Genet. **71:**68–76.
16. **Cutt, J. R., T. Shenk, and P. Hearing.** 1987. Analysis of adenovirus early region 4-encoded polypeptides synthesized in productively infected cells. J. Virol. **61:**543–552.
17. **Dobbelstein, M., J. Roth, W. T. Kimberly, A. J. Levine, and T. Shenk.** 1997. Nuclear export of the E1B 55-kDa and E4 34-kDa adenoviral oncoproteins mediated by a rev-like signal sequence. EMBO J. **16:**4276–4284.
18. **Dosch, T., F. Horn, G. Schneider, F. Kratzer, T. Dobner, J. Hauber, and R. H. Stauber.** 2001. The adenovirus type 5 E1B-55K oncoprotein actively shuttles in virus-infected cells, whereas transport of E4orf6 is mediated by a CRM1-independent mechanism. J. Virol. **75:**5677–5683.
19. **Fleisig, H. B., N. I. Orazio, H. Liang, A. F. Tyler, H. P. Adams, M. D. Weitzman, and L. Nagarajan.** 2007. Adenoviral E1B55K oncoprotein sequesters candidate leukemia suppressor sequence-specific single-stranded DNA-binding protein 2 into aggresomes. Oncogene **26:**4797–4805.
20. **Flint, S. J., and R. A. Gonzalez.** 2003. Regulation of mRNA production by the adenoviral E1B 55-kDa and E4 Orf6 proteins. Curr. Top. Microbiol. Immunol. **272:**287–330.
21. **Fuerst, T. R., E. G. Niles, F. W. Studier, and B. Moss.** 1986. Eukaryotic transient-expression system based on recombinant vaccinia virus that synthesizes bacteriophage T7 RNA polymerase. Proc. Natl. Acad. Sci. USA **83:**8122–8126.
22. **Fujita, Y., M. Nishimura, M. Taniwaki, T. Abe, and T. Okuda.** 2001. Identification of an alternatively spliced form of the mouse AML1/RUNX1 gene transcript AML1c and its expression in early hematopoietic development. Biochem. Biophys. Res. Commun. **281:**1248–1255.
23. **Garnett, C. T., D. Erdman, W. Xu, and L. R. Gooding.** 2002. Prevalence and quantitation of species C adenovirus DNA in human mucosal lymphocytes. J. Virol. **76:**10608–10616.
24. **Gonzalez, R., W. Huang, R. Finnen, C. Bragg, and S. J. Flint.** 2006. Adenovirus E1B 55-kilodalton protein is required for both regulation of mRNA export and efficient entry into the late phase of infection in normal human fibroblasts. J. Virol. **80:**964–974.
25. **Gonzalez, R. A., and S. J. Flint.** 2002. Effects of mutations in the adenoviral E1B 55-kilodalton protein coding sequence on viral late mRNA metabolism. J. Virol. **76:**4507–4519.
26. **Goodrum, F. D., T. Shenk, and D. A. Ornelles.** 1996. Adenovirus early region 4 34-kilodalton protein directs the nuclear localization of the early region 1B 55-kilodalton protein in primate cells. J. Virol. **70:**6323–6335.
27. **Graw, S. L., K. Gardiner, K. Hall-Johnson, I. Hart, A. Joetham, K. Walton, D. Donaldson, and D. Patterson.** 1995. Molecular analysis and breakpoint definition of a set of human chromosome 21 somatic cell hybrids. Somat. Cell Mol. Genet. **21:**415–428.
28. **Gustafsson, B., W. Huang, G. Bogdanovic, F. Gauffin, A. Nordgren, G. Talekar, D. A. Ornelles, and L. R. Gooding.** 2007. Adenovirus DNA is detected at increased frequency in Guthrie cards from children who develop acute lymphoblastic leukaemia. Br. J. Cancer **97:**992–994.
29. **Halbert, D. N., J. R. Cutt, and T. Shenk.** 1985. Adenovirus early region 4 encodes functions required for efficient DNA replication, late gene expression, and host cell shutoff. J. Virol. **56:**250–257.
30. **Harada, J. N., A. Shevchenko, A. Shevchenko, D. C. Pallas, and A. J. Berk.** 2002. Analysis of the adenovirus E1B-55K-anchored proteome reveals its link to ubiquitination machinery. J. Virol. **76:**9194–9206.
31. **Harrington, K. S., A. Javed, H. Drissi, S. McNeil, J. B. Lian, J. L. Stein, A. J. Van Wijnen, Y. L. Wang, and G. S. Stein.** 2002. Transcription factors RUNX1/AML1 and RUNX2/Cbfa1 dynamically associate with stationary subnuclear domains. J. Cell Sci. **115:**4167–4176.
32. **Huang, M. M., and P. Hearing.** 1989. Adenovirus early region 4 encodes two gene products with redundant effects in lytic infection. J. Virol. **63:**2605–2615.
33. **Ito, Y.** 1999. Molecular basis of tissue-specific gene expression mediated by the runt domain transcription factor PEBP2/CBF. Genes Cells **4:**685–696.
34. **Ito, Y.** 2004. Oncogenic potential of the RUNX gene family: overview. Oncogene **23:**4198–4208.
35. **Ito, Y.** 2008. RUNX genes in development and cancer: regulation of viral gene expression and the discovery of RUNX family genes. Adv. Cancer Res. **99C:**33–76.
36. **Javed, A., B. Guo, S. Hiebert, J. Y. Choi, J. Green, S. C. Zhao, M. A. Osborne, S. Stifani, J. L. Stein, J. B. Lian, A. J. van Wijnen, and G. S. Stein.** 2000. Groucho/TLE/R-esp proteins associate with the nuclear matrix and repress RUNX (CBFα/AML/PEBP2α) dependent activation of tissue-specific gene transcription. J. Cell Sci. **113:**2221–2231.
37. **Jones, N., and T. Shenk.** 1979. Isolation of adenovirus type 5 host range deletion mutants defective for transformation of rat embryo cells. Cell **17:**683–689.
38. **Kamachi, Y., E. Ogawa, M. Asano, S. Ishida, Y. Murakami, M. Satake, Y. Ito, and K. Shigesada.** 1990. Purification of a mouse nuclear factor that binds to both the A and B cores of the polyomavirus enhancer. J. Virol. **64:**4808–4819.
39. **Kitabayashi, I., A. Yokoyama, K. Shimizu, and M. Ohki.** 1998. Interaction and functional cooperation of the leukemia-associated factors AML1 and p300 in myeloid cell differentiation. EMBO J. **17:**2994–3004.
40. **König, C., J. Roth, and M. Dobbelstein.** 1999. Adenovirus type 5 E4orf3

protein relieves p53 inhibition by E1B-55-kilodalton protein. J. Virol. **73:** 2253–2262.

41. **Krätzer, F., O. Rosorius, P. Heger, N. Hirschmann, T. Dobner, J. Hauber, and R. H. Stauber.** 2000. The adenovirus type 5 E1B-55K oncoprotein is a highly active shuttle protein and shuttling is independent of E4orf6, p53 and Mdm2. Oncogene **19:**850–857.
42. **Leppard, K. N., and R. D. Everett.** 1999. The adenovirus type 5 E1b 55K and E4 Orf3 proteins associate in infected cells and affect ND10 components. J. Gen. Virol. **80:**997–1008.
43. **Lethbridge, K. J., G. E. Scott, and K. N. Leppard.** 2003. Nuclear matrix localization and SUMO-1 modification of adenovirus type 5 E1b 55K protein are controlled by E4 Orf6 protein. J. Gen. Virol. **84:**259–268.
44. **Levanon, D., G. Glusman, T. Bangsow, E. Ben-Asher, D. A. Male, N. Avidan, C. Bangsow, M. Hattori, T. D. Taylor, S. Taudien, K. Blechschmidt, N. Shimizu, A. Rosenthal, Y. Sakaki, D. Lancet, and Y. Groner.** 2001. Architecture and anatomy of the genomic locus encoding the human leukemia-associated transcription factor RUNX1/AML1. Gene **262:**23–33.
45. **Levanon, D., R. E. Goldstein, Y. Bernstein, H. Tang, D. Goldenberg, S. Stifani, Z. Paroush, and Y. Groner.** 1998. Transcriptional repression by AML1 and LEF-1 is mediated by the TLE/Groucho corepressors. Proc. Natl. Acad. Sci. USA **95:**11590–11595.
46. **Liu, Y., A. Shevchenko, A. Shevchenko, and A. J. Berk.** 2005. Adenovirus exploits the cellular aggresome response to accelerate inactivation of the MRN complex. J. Virol. **79:**14004–14016.
47. **Lutterbach, B., J. J. Westendorf, B. Linggi, S. Isaac, E. Seto, and S. W. Hiebert.** 2000. A mechanism of repression by acute myeloid leukemia-1, the target of multiple chromosomal translocations in acute leukemia. J. Biol. Chem. **275:**651–656.
48. **Martinez-Palomo, A.** 1968. Ultrastructural study of the replication of human adenovirus type 12 in cultured cells. Pathol. Microbiol. **31:**147–164.
49. **Martinez-Palomo, A., and N. Granboulan.** 1967. Electron microscopy of adenovirus 12 replication. II. High-resolution autoradiography of infected KB cells labeled with tritiated thymidine. J. Virol. **1:**1010–1018.
50. **Marton, M. J., S. B. Baim, D. A. Ornelles, and T. Shenk.** 1990. The adenovirus E4 17-kilodalton protein complexes with the cellular transcription factor E2F, altering its DNA-binding properties and stimulating E1A-independent accumulation of E2 mRNA. J. Virol. **64:**2345–2359.
51. **McNees, A. L., C. T. Garnett, and L. R. Gooding.** 2002. The adenovirus E3 RID complex protects some cultured human T and B lymphocytes from Fas-induced apoptosis. J. Virol. **76:**9716–9723.
52. **McNees, A. L., J. A. Mahr, D. Ornelles, and L. R. Gooding.** 2004. Postinternalization inhibition of adenovirus gene expression and infectious virus production in human T-cell lines. J. Virol. **78:**6955–6966.
53. **Meyers, S., and S. W. Hiebert.** 1995. Indirect and direct disruption of transcriptional regulation in cancer: E2F and AML-1. Crit. Rev. Eukaryot. Gene Expr. **5:**365–383.
54. **Miyoshi, H., M. Ohira, K. Shimizu, K. Mitani, H. Hirai, T. Imai, K. Yokoyama, E. Soeda, and M. Ohki.** 1995. Alternative splicing and genomic structure of the AML1 gene involved in acute myeloid leukemia. Nucleic Acids Res. **23:**2762–2769.
55. **Murakami, Y., L. F. Chen, N. Sanechika, H. Kokuzaki, and Y. Ito.** 2007. Transcription factor Runx1 recruits the polyomavirus replication origin to replication factories. J. Cell Biochem. **100:**1313–1323.
56. **Ogawa, E., M. Maruyama, H. Kagoshima, M. Inuzuka, J. Lu, M. Satake, K. Shigesada, and Y. Ito.** 1993. PEBP2/PEA2 represents a family of transcription factors homologous to the products of the Drosophila runt gene and the human AML1 gene. Proc. Natl. Acad. Sci. USA **90:**6859–6863.
57. **Orlando, J. S., and D. A. Ornelles.** 1999. An arginine-faced amphipathic alpha helix is required for adenovirus type 5 e4orf6 protein function. J. Virol. **73:**4600–4610.
58. **Orlando, J. S., and D. A. Ornelles.** 2002. E4orf6 variants with separate abilities to augment adenovirus replication and direct nuclear localization of the E1B 55-kilodalton protein. J. Virol. **76:**1475–1487.
59. **Orlicky, D. J., J. DeGregori, and J. Schaack.** 2001. Construction of stable coxsackievirus and adenovirus receptor-expressing 3T3-L1 cells. J. Lipid Res. **42:**910–915.
60. **Ornelles, D. A., and T. Shenk.** 1991. Localization of the adenovirus early region 1B 55-kilodalton protein during lytic infection: association with nuclear viral inclusions requires the early region 4 34-kilodalton protein. J. Virol. **65:**424–429.
61. **Pérez-Alvarado, G. C., M. Martinez-Yamout, M. M. Allen, R. Grosschedl, H. J. Dyson, and P. E. Wright.** 2003. Structure of the nuclear factor ALY: insights into post-transcriptional regulatory and mRNA nuclear export processes. Biochemistry **42:**7348–7357.
62. **Perry, C., A. Eldor, and H. Soreq.** 2002. Runx1/AML1 in leukemia: disrupted association with diverse protein partners. Leuk. Res. **26:**221–228.
63. **Pilder, S., M. Moore, J. Logan, and T. Shenk.** 1986. The adenovirus E1B-55K transforming polypeptide modulates transport or cytoplasmic stabilization of viral and host cell mRNAs. Mol. Cell. Biol. **6:**470–476.
64. **Pombo, A., J. Ferreira, E. Bridge, and M. Carmo-Fonseca.** 1994. Adenovirus replication and transcription sites are spatially separated in the nucleus of infected cells. EMBO J. **13:**5075–5085.
65. **Pozner, A., D. Goldenberg, V. Negreanu, S. Y. Le, O. Elroy-Stein, D. Levanon, and Y. Groner.** 2000. Transcription-coupled translation control of AML1/RUNX1 is mediated by cap- and internal ribosome entry site-dependent mechanisms. Mol. Cell. Biol. **20:**2297–2307.
66. **Puvion-Dutilleul, F., and E. Puvion.** 1990. Analysis by in situ hybridization and autoradiography of sites of replication and storage of single- and double-stranded adenovirus type 5 DNA in lytically infected HeLa cells. J. Struct. Biol. **103:**280–289.
67. **Querido, E., P. Blanchette, Q. Yan, T. Kamura, M. Morrison, D. Boivin, W. G. Kaelin, R. C. Conaway, J. W. Conaway, and P. E. Branton.** 2001. Degradation of p53 by adenovirus E4orf6 and E1B55K proteins occurs via a novel mechanism involving a Cullin-containing complex. Genes Dev. **15:** 3104–3117.
68. **Querido, E., R. C. Marcellus, A. Lai, R. Charbonneau, J. G. Teodoro, G. Ketner, and P. E. Branton.** 1997. Regulation of p53 levels by the E1B 55-kilodalton protein and E4orf6 in adenovirus-infected cells. J. Virol. **71:** 3788–3798.
69. **Rasband, W. S.** 2007. ImageJ, version 1.38q ed. National Institutes of Health, Bethesda, MD.
70. **Reich, N. C., P. Sarnow, E. Duprey, and A. J. Levine.** 1983. Monoclonal antibodies which recognize native and denatured forms of the adenovirus DNA-binding protein. Virology **128:**480–484.
71. **Sandler, A. B., and G. Ketner.** 1989. Adenovirus early region 4 is essential for normal stability of late nuclear RNAs. J. Virol. **63:**624–630.
72. **Sarnow, P., P. Hearing, C. W. Anderson, D. N. Halbert, T. Shenk, and A. J. Levine.** 1984. Adenovirus early region 1B 58,000-dalton tumor antigen is physically associated with an early region 4 25,000-dalton protein in productively infected cells. J. Virol. **49:**692–700.
73. **Satake, M., M. Inuzuka, K. Shigesada, T. Oikawa, and Y. Ito.** 1992. Differential expression of subspecies of polyomavirus and murine leukemia virus enhancer core binding protein, PEBP2, in various hematopoietic cells. Jpn. J. Cancer Res. **83:**714–722.
74. **Schmidt, H. M., G. Steger, and H. Pfister.** 1997. Competitive binding of viral E2 protein and mammalian core-binding factor to transcriptional control sequences of human papillomavirus type 8 and bovine papillomavirus type 1. J. Virol. **71:**8029–8034.
75. **Speck, N. A., T. Stacy, Q. Wang, T. North, T. L. Gu, J. Miller, M. Binder, and M. Marin-Padilla.** 1999. Core-binding factor: a central player in hematopoiesis and leukemia. Cancer Res. **59:**1789s–1793s.
76. **Speck, N. A., and S. Terryl.** 1995. A new transcription factor family associated with human leukemias. Crit. Rev. Eukaryot. Gene Expr. **5:**337–364.
77. **Steegenga, W. T., N. Riteco, A. G. Jochemsen, F. J. Fallaux, and J. L. Bos.** 1998. The large E1B protein together with the E4orf6 protein target p53 for active degradation in adenovirus infected cells. Oncogene **16:**349–357.
78. **Stracker, T. H., C. T. Carson, and M. D. Weitzman.** 2002. Adenovirus oncoproteins inactivate the Mre11-Rad50-NBS1 DNA repair complex. Nature **418:**348–352.
79. **Sutton, K. A., C. T. Lin, G. D. Harkiss, I. McConnell, and D. R. Sargan.** 1997. Regulation of the long terminal repeat in visna virus by a transcription factor related to the AML/PEBP2/CBF superfamily. Virology **229:** 240–250.
80. **Tsuzuki, S., D. Hong, R. Gupta, K. Matsuo, M. Seto, and T. Enver.** 2007. Isoform-specific potentiation of stem and progenitor cell engraftment by AML1/RUNX1. PLoS Med. **4:**e172.
81. **Voelkerding, K., and D. F. Klessig.** 1986. Identification of two nuclear subclasses of the adenovirus type 5-encoded DNA-binding protein. J. Virol. **60:**353–362.
82. **Weitzman, M. D., and D. A. Ornelles.** 2005. Inactivating intracellular antiviral responses during adenovirus infection. Oncogene **24:**7686–7696.
83. **Woo, J. L., and A. J. Berk.** 2007. Adenovirus ubiquitin-protein ligase stimulates viral late mRNA nuclear export. J. Virol. **81:**575–587.
84. **Zaiman, A. L., and J. Lenz.** 1996. Transcriptional activation of a retrovirus enhancer by CBF (AML1) requires a second factor: evidence for cooperativity with c-Myb. J. Virol. **70:**5618–5629.
85. **Zaiman, A. L., A. F. Lewis, B. E. Crute, N. A. Speck, and J. Lenz.** 1995. Transcriptional activity of core binding factor-alpha (AML1) and beta subunits on murine leukemia virus enhancer cores. J. Virol. **69:**2898–2906.
86. **Zantema, A., J. A. Fransen, A. Davis-Olivier, F. C. Ramaekers, G. P. Vooijs, B. DeLeys, and A. J. Van der Eb.** 1985. Localization of the E1B proteins of adenovirus 5 in transformed cells, as revealed by interaction with monoclonal antibodies. Virology **142:**44–58.
87. **Zeng, C., S. McNeil, S. Pockwinse, J. Nickerson, L. Shopland, J. B. Lawrence, S. Penman, S. Hiebert, J. B. Lian, A. J. van Wijnen, J. L. Stein, and G. S. Stein.** 1998. Intranuclear targeting of AML/CBFα regulatory factors to nuclear matrix-associated transcriptional domains. Proc. Natl. Acad. Sci. USA **95:**1585–1589.

88. **Zhang, Y. W., S. C. Bae, G. Huang, Y. X. Fu, J. Lu, M. Y. Ahn, Y. Kanno, T. Kanno, and Y. Ito.** 1997. A novel transcript encoding an N-terminally truncated AML1/PEBP2 αB protein interferes with transactivation and blocks granulocytic differentiation of 32Dcl3 myeloid cells. Mol. Cell. Biol. **17**:4133–4145.
89. **Zhang, Y. W., N. Yasui, K. Ito, G. Huang, M. Fujii, J. Hanai, H. Nogami, T. Ochi, K. Miyazono, and Y. Ito.** 2000. A RUNX2/PEBP2alpha A/CBFA1 mutation displaying impaired transactivation and Smad interaction in cleidocranial dysplasia. Proc. Natl. Acad. Sci. USA **97**:10549–10554.
90. **Zhou, Z., M. J. Luo, K. Straesser, J. Katahira, E. Hurt, and R. Reed.** 2000. The protein Aly links pre-messenger-RNA splicing to nuclear export in metazoans. Nature **407**:401–405.

THE JOURNAL OF BIOLOGICAL CHEMISTRY VOL. 283, NO. 36, pp. 24420–24425, September 5, 2008

Acetylation of PML Is Involved in Histone Deacetylase Inhibitor-mediated Apoptosis*[S]

Received for publication, March 20, 2008, and in revised form, July 7, 2008 Published, JBC Papers in Press, July 11, 2008, DOI 10.1074/jbc.M802217200

Fumihiko Hayakawa[‡1], **Akihiro Abe**[‡], **Issay Kitabayashi**[§], **Pier Paolo Pandolfi**[¶], **and Tomoki Naoe**[‡]

From the [‡]*Department of Hematology and Oncology, Nagoya University, Graduate School of Medicine, Nagoya 466-8550, Japan, the* [§]*Molecular Oncology Division, National Cancer Center Research Institute, 5-1-1 Tsukiji, Chuo-ku, Tokyo 104-0045, Japan, and the* [¶]*Cancer Genetics Program, Beth Israel Deaconess Cancer Center, Department of Medicine, Harvard Medical School, Boston, Massachusetts 02215*

PML is a potent tumor suppressor and proapoptotic factor and is functionally regulated by post-translational modifications such as phosphorylation, sumoylation, and ubiquitination. Histone deacetylase (HDAC) inhibitors are a promising class of targeted anticancer agents and induce apoptosis in cancer cells by largely unknown mechanisms. We report here a novel post-transcriptional modification, acetylation, of PML. PML exists as an acetylated protein in HeLa cells, and its acetylation is enhanced by coexpression of p300 or treatment with a HDAC inhibitor, trichostatin A. Increased PML acetylation is associated with increased sumoylation of PML *in vitro* and *in vivo*. PML is involved in trichostatin A-induced apoptosis and PML with an acetylation-defective mutation shows an inability to mediate apoptosis, suggesting the importance of PML acetylation. Our work provides new insights into PML regulation by post-translational modification and new information about the therapeutic mechanism of HDAC inhibitors.

The promyelocytic leukemia protein PML controls cell cycle progression, senescence, and cell death (1, 2). Wild-type PML is a potent growth suppressor that, when overexpressed, can block cell cycle progression in a variety of tumor cell lines (1); conversely $PML^{-/-}$ mouse embryo fibroblasts (MEFs)[2] replicate significantly faster than their $PML^{+/+}$ MEFs (3). PML also plays an essential role in DNA damage or stress-induced apoptosis, and $PML^{-/-}$ cells are resistant to a variety of apoptotic signals (4). In normal cells, the PML protein is localized in, and essential for the biogenesis of, discrete subnuclear compartments designated as nuclear bodies (NBs) (5). In NBs, PML coaccumulates with more than 70 kinds of proteins that are involved in tumor suppression, apoptosis, regulation of gene expression, anti-viral response, and DNA repair. PML is thought to exert its function by regulating the function of binding partners as a core of NBs (6). Intriguingly, NBs are disrupted in human acute promyelocytic leukemia cells by PML-RARα, a oncogenic fusion protein of PML, and RAR-α, which is thought to be the mechanism of anti-apoptotic effect of PML-RARα (7–9).

It has been reported that NB formation requires PML to be conjugated to SUMO-1 (5, 10). SUMO-1 is an 11-kDa protein that is structurally homologous to ubiquitin (11). Sumoylation is thought to regulate the subcellular localization, stability, DNA binding, and/or transcriptional ability of its target proteins such as PML, Ran GTPase-activating protein (RanGAP)1, IκBα, and heat shock transcription factor 2 (11). Virtually As_2O_3, a chemotherapeutic agent clinically used in the treatment of acute promyelocytic leukemia cells, induces PML sumoylation. Increased PML sumoylation induced by As_2O_3 treatment leads to the restoration of NBs disrupted by PML-RARα and then is followed by apoptosis in acute promyelocytic leukemia cells, which results in prolonged remission of the disease (12–15). These findings underscore the importance of PML sumoylation and the integrity of NBs to tumor suppression.

Histone deacetylase (HDAC) inhibitors, a promising class of targeted anticancer agents, can block proliferation and induce cell death in a wide variety of transformed cells (16). HDAC inhibitors block the activity of class I and II HDACs and induce histone acetylation, which leads to the relaxation of chromatin structure, enhanced accessibility of transcription machinery to DNA, and increased gene transcription (17). HDAC inhibitors also induce acetylation of transcription factors, which alters their activities and the expression of their target genes (18). Recent studies demonstrated that p53 acetylation induced by a HDAC inhibitor leads to expression of proapoptotic proteins such as Bax, PIG3, and NOXA (19, 20). However, the mechanisms of p53-independent apoptosis by HDAC inhibitor remain largely unknown.

Here, we report PML acetylation as its novel post-transcriptional modification. PML acetylation is induced by trichostatin A (TSA), a HDAC inhibitor. This enhanced acetylation leads to increased PML sumoylation and may play a key role in TSA-induced apoptosis. This work provides new insights into the

* This work was supported by grants-in-aid from the Uehara Memorial Foundation, the National Institute of Biomedical Innovation, and the Ministry of Education, Culture, Sports, Science, and Technology of Japan. The costs of publication of this article were defrayed in part by the payment of page charges. This article must therefore be hereby marked "*advertisement*" in accordance with 18 U.S.C. Section 1734 solely to indicate this fact.

[S] The on-line version of this article (available at http://www.jbc.org) contains supplemental Fig. S1–S9 and supplemental data.

[1] To whom correspondence should be addressed: Dept. of Hematology and Oncology, Nagoya University, Graduate School of Medicine, 65 Tsurumai-cho, Showa-ku, Nagoya, 466-8550, Japan. Fax: 81-52-744-2161; E-mail: bun-hy@med.nagoya-u.ac.jp.

[2] The abbreviations used are: MEF, mouse embryo fibroblast; HDAC, histone deacetylase; TSA, trichostatin A; NB, nuclear body; RAR, retinoic acid receptor; SUMO, small ubiquitin-like modifier; HAT, histone acetyltransferase; GST, glutathione *S*-transferase; HA, hemagglutinin; GFP, green fluorescent protein.

functional regulation of PML and the therapeutic mechanisms of treatment with HDAC inhibitors.

EXPERIMENTAL PROCEDURES

Antibodies, Plasmids, and Cell Culture—The sources of antibodies and plasmids and the cell culture conditions are detailed in the supplemental data.

Transient Transfection, Immunoprecipitation, Immunoblotting, Immunofluorescence, and in Vitro and in Vivo Acetylation Assays—These were performed as described previously (21, 28) except transient transfections into PML$^{-/-}$ MEFs were performed by nucleofection using the Nucleofector system (Amaxa Biosystems) according to the manufacturer's instructions.

Antibody Array Assay and Detection and Quantification of Apoptosis—These are also detailed in the supplemental data.

In Vitro Sumoylation Assay—The *in vitro* sumoylation assay was performed essentially as described previously (21), except recombinant SUMO E1 ligase purchased from BIOMOL International was used instead of HeLa cell lysate.

Cell Sorting—Cell sorting was performed using BD FACSAria Cell Sorter (BD Biosciences) according to the manufacturer's instructions.

RESULTS

PML Exists as an Acetylated Protein in HeLa Cells Treated with Trichostatin A—HDAC inhibitors including TSA induce differentiation, growth arrest, and apoptosis of cancer cells. In addition to their effects on histones, HDAC inhibitors increase the acetylation level of several non-histone proteins, such as transcription factors, cytoskeletal proteins, and molecular chaperones, which are important for their effects on cancer cells (18). These observations prompted us to screen new acetylation targets of TSA with an antibody array assay combined with *in vivo* labeling of acetylated proteins with [^{14}C]acetate. Seven spots indicating possible targets of TSA-induced acetylation were detected (supplemental Fig. S1 and Fig. 1*A*). We focused on one of these targets, PML, a multifunctional protein that is involved in apoptosis, tumor suppression, and cell cycle regulation (2). We set out to confirm whether PML was acetylated *in vivo*. The same anti-PML antibody as used in the antibody array assay immunoprecipitated an ~79-kDa acetylated protein from lysates of TSA-treated HeLa cells (Fig. 1*B*), suggesting that PML existed as an acetylated protein in them. Of note, the antibody we used detected only a single band of PML, although PML has seven isoforms. The antibody was confirmed to be able to detect all PML isoforms, suggesting that this PML was the main one expressed in HeLa cells (supplemental Fig. S1).

PML Is Acetylated by p300 and GCN5 in Vitro—To test whether known histone acetyltransferases (HATs), p300 and GSN5, can acetylate PML, we performed an *in vitro* acetylation assay using GST-PML as a substrate. Both HATs acetylated PML *in vitro* (Fig. 2*A*), and we focused on the acetylation by p300 that occurred with higher efficiency. Use of a series of PML subdomains in the *in vitro* p300 acetylation assay indicated that PML would be acetylated on the C-terminal domain, amino acids 448–560 (supplemental Fig. S2). Inspection of the

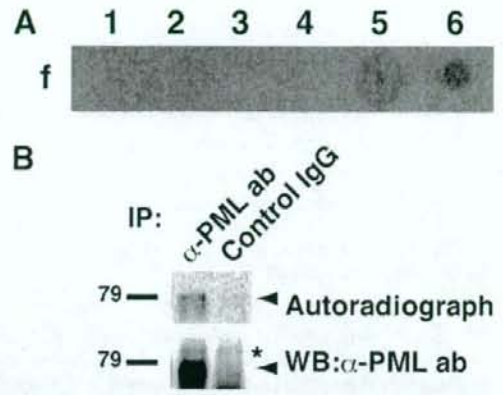

FIGURE 1. **PML exists as an acetylated protein in HeLa cells treated with TSA.** *A*, screening for acetylation targets of TSA by antibody array. Lysate from HeLa cells pulse-labeled with [^{14}C]acetate and treated with TSA was incubated with a nitrocellulose array comprising 113 antibodies. After extensive washes, the array was subjected to autoradiography. Similar results were obtained from duplicated experiments. Representative spots are shown. The antibodies used for *f-1* to *f-6* are anti-MEK1/2 antibody, anti-phospho-MEK1/2 antibody, anti-MKP-1 (V-15) antibody, anti-PML (PG-M) antibody, anti-PML (H-238) antibody, and anti-acetylated lysine antibody, respectively. *B*, PML exists as an acetylated protein in TSA-treated HeLa cells. Pulse-labeled HeLa cells with TSA treatment were lysed as in *A*. The lysates were immunoprecipitated (*IP*) with PML antibody (*ab*) or control rabbit IgG. 90% of the immunoprecipitates were subjected to SDS-PAGE, autoradiography, and detection with phosphorimaging (*upper panel*). 10% of the immunoprecipitates were subjected to SDS-PAGE and immunoblotting with PML antibody (*lower panel*). The positions of PML and nonspecific band are indicated by an *arrow* and an *asterisk*, respectively. *WB*, Western blotting.

PML sequence in this region revealed the presence of 7 lysine residues (supplemental Fig. S2); therefore, we introduced a series of arginine substitutions to map the acetylation sites. Within the C-terminal domain of PML, only the substitution of arginine for lysine 487 (K487R) measurably reduced acetylation of PML by p300 among all the individual substitutions (Fig. 2*B*; mutations are designated by the codon number between Lys and Arg). When arginine substitutions for other lysines were combined with K487R, a further reduction of acetylation was observed with K515R (Fig. 2*C*). Acetylation of full-length PML was impaired by substitutions of K487R and K487R/K515R similarly to that of the C-terminal domain of PML (Fig. 2*D*). Our results indicate that the principal sites of p300 acetylation in PML will be lysines 487 and 515.

PML Acetylation Is Increased in Response to TSA Treatment—We examined whether PML acetylation by p300 occurred *in vivo* at the same sites as identified *in vitro*. Wild-type PML and PML with the K487R/K515R mutations were designated as PML W and PML M, respectively. Coexpression of p300 enhanced PML W acetylation, whereas acetylation PML M was weak in the basal state and showed no significant response to p300 coexpression (Fig. 3*A*, *top panel*). The efficiency of immunoprecipitation was the same for all samples (Fig. 3*A*, *middle panel*), and the increase in acetylation of a 17-kDa protein by coexpression of p300, which suggested the induction of histone acetylation, was equal between transfectants with PML W and PML M (Fig. 3*A*, *bottom panel*). These results suggest that p300 acetylates PML *in vivo* at the same sites as identified *in vitro*.

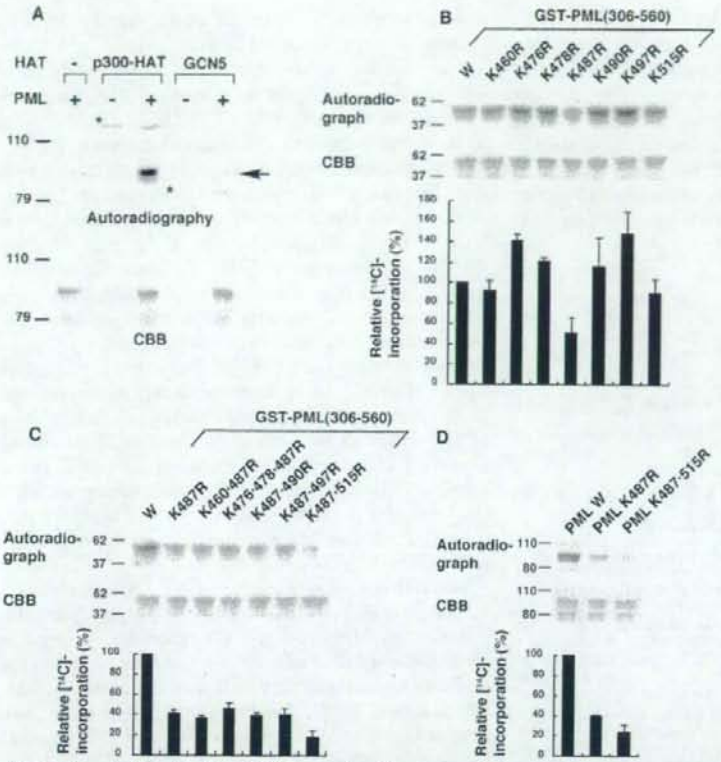

FIGURE 2. **PML acetylation *in vitro*.** *A*, PML is acetylated by p300 and GCN5. GST-PML was incubated with [^{14}C]acetyl-CoA and the indicated HATs. The reaction mixtures were subjected to SDS-PAGE, Coomassie Brilliant Blue (*CBB*) staining, and autoradiography. The positions of acetylated PML and acetylases are indicated by an *arrow* and *asterisks*, respectively. *B* and *C*, identification of PML acetylation sites. Wild-type or mutant GST-PML (amino acids 306–560) were subjected to *in vitro* acetylation by p300-HAT as in *A*. ^{14}C incorporation into each GST-PML construct was quantified using phosphorimaging. A representative phosphorimaging scan (*top panel*), the corresponding CBB-stained electrophoretogram (*middle panel*), and the quantitation of the ^{14}C incorporation for each mutant, relative to the wild-type PML construct (*bottom panel*), are presented. The averages of three independent analyses and standard deviations are shown. *D*, mutation of lysines in full-length PML reduced acetylation by p300. Wild-type or mutant GST-PML (full-length) were subjected to *in vitro* acetylation assays as described in *B*.

Next, we tested whether PML acetylation is induced by TSA. Similarly to the case of p300 coexpression, TSA treatment enhanced PML W acetylation, whereas acetylation of PML M was significantly reduced and showed no significant response to TSA treatment (Fig. 3*B*, *top panel*). Our results suggest that PML is an acetylation target of TSA and that PML acetylation in response to TSA largely occurs at the sites of acetylation by p300.

Acetylation of PML in Response to TSA Is Associated with Enhanced PML Sumoylation—Because one of the PML acetylation sites, lysine 487, is located in the putative nuclear localization signal (amino acids 476–490), we first examined whether PML acetylation affected its nuclear localization to see the effect of acetylation on PML function. However, TSA treatment and the acetylation-defective mutation did not obviously affect PML nuclear localization or accumulation to NBs in immunofluorescent staining (supplemental Fig. S3). We next investigated whether PML acetylation affected its sumoylation, which is required for PML to exercise many of its functions. We set up an *in vivo* sumoylation system in which conjugation of SUMO to PML could be detected by Western analysis, resulting in the appearance of a novel 100-kDa protein expected to be sumoylated PML (21). In this system, coexpression of p300 and exposure to TSA resulted in a significant increase in sumoylation of PML W, whereas sumoylation of PML M was weak and not obviously affected by these treatments (Fig. 4, *A* and *B*). These results suggest the possibility that PML acetylation at lysines 487 and 515 enhances its sumoylation. Next, to verify that acetylated PML is directly sumoylated, we set up an *in vitro* sumoylation system in which recombinant HA-tagged PML protein was incubated with recombinant SUMO E1 and E2 ligase and SUMO with or without a prior acetylation reaction using [^{14}C]acetyl-CoA. Autoradiography visualizing only acetylated PML demonstrated that acetylated PML was efficiently sumoylated (Fig. 4*C*, *upper panel*). Of note, sumoylation efficiency observed in the autoradiograph was much higher than that in immunoblotting with anti-HA antibody where acetylated and nonacetylated PML were visualized (Fig. 4*C*, *upper panel*, *lane 2 versus lower panel*, *lane 2*). These results indicate that acetylated PML may be preferentially sumoylated *in vitro*.

PML Acetylation May Play an Important Role in TSA-induced Apoptosis—TSA treatment induces apoptosis in HeLa cells by unknown mechanisms (16). In our previous study, PML sumoylation plays an important role in As_2O_3-induced apoptosis (21). Given our findings that PML acetylation is associated with increased PML sumoylation, this may represent one of the mechanisms of TSA-induced apoptosis. We first examined whether PML was involved in TSA-induced apoptosis. For this purpose, we established HeLa cells stably transfected with an expression vector for small hairpin RNA against PML and an empty control vector and designated them as PML KD HeLa and control KD HeLa, respectively. Successful knocking down of PML was confirmed by immunofluorescence analysis with an anti-PML antibody (supplemental Fig. S4). TSA treatment caused the appearance of a sub-G_1 peak in cell cycle analysis, a marker of apoptosis, in both cells. However, the ratio of apoptotic cells was reduced by ~60% in PML KD HeLa compared with control KD HeLa, suggesting the involvement of PML in

TSA-induced apoptosis (Fig. 5*A* and supplemental Fig. S5). We examined further using PML$^{-/-}$ MEFs. Notably, overexpression of PML W in PML$^{-/-}$ MEFs substantially increased TSA-induced apoptosis relative to cells transfected with an empty vector, whereas, PML M displayed an impaired ability to mediate apoptosis in response to TSA (Fig. 5*B* and supplemental Fig. S6). An equal expression level of PML between PML W and PML M transfectants was confirmed (supplemental Fig. S6). These results further support the involvement of PML in TSA-induced apoptosis and suggest the importance of PML acetylation in conferring apoptosis by TSA.

Next, we investigated the effect of PML sumoylation on PML-mediated apoptosis in response to TSA. Cotransfection of expression vectors for SUMO and Ubc9 further sensitized PML W transfectants to TSA-induced apoptosis (Fig. 5*C*, *third* and *fourth lanes*), whereas the proapoptotic effects of SUMO and Ubc9 were greatly reduced in control and PML M transfectants (Fig. 5*C*, *first* and *second lanes* and *fifth* and *sixth lanes*). Enhanced sumoylation of PML W induced by TSA and impaired sumoylation of PML M were observed also in PML$^{-/-}$ MEFs (Fig. 5*D*). These results suggest that sumoylation enhances PML-mediated apoptosis in response to TSA. To test this hypothesis, we created an expression vector for the PML-3K mutant, which had lysine-to-arginine mutations at all three PML sumoylation sites and cannot be sumoylated (22). Overexpression of PML-3K in either the presence or absence of SUMO and Ubc9 had little or no effect on TSA-induced apoptosis (Fig. 5*C*, *seventh* and *eighth lanes*), indicative of a requirement for PML sumoylation in TSA-mediated apoptosis. These results suggest the hypothesis that enhanced PML sumoylation through PML acetylation is one of the mechanisms of TSA-induced apoptosis.

Finally, to investigate the generality of the effects of TSA on PML among HDAC inhibitors, we used depsipeptide, another HDAC inhibitor that belongs to a different class. Depsipeptide enhanced acetylation and sumoylation of PML, and its apoptotic effect was increased by PML expression similarly to TSA (supplemental Fig. S8). These results further support the hypothetical importance of PML acetylation in HDAC inhibitor-induced apoptosis.

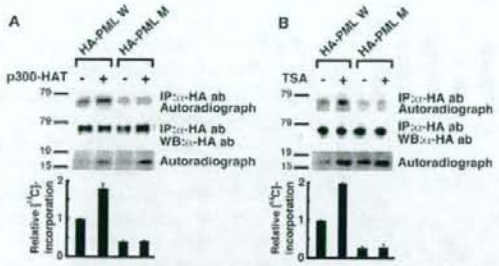

FIGURE 3. **PML acetylation *in vivo*.** *A*, PML acetylation is induced by p300 cotransfection *in vivo*. HeLa cells were transfected with indicated expression vectors. PML acetylation was analyzed as in Fig. 1*B* except for the use of anti-HA antibody (*ab*) instead of anti-PML antibody for IP and IB. The lysates were also subjected to SDS-PAGE followed by autoradiography to confirm successful induction of histone acetylation by p300-HAT cotransfection. A representative autoradiograph of PML (*top panel*), the corresponding image of IB with anti-HA antibody (*second panel from the top*), and the autoradiograph of histone (*third panel from the top*) are presented. ^{14}C incorporation into PML and the amount of immunoprecipitated (*IP*) PML protein were quantified using analyzer of each imaging system. Relative ^{14}C incorporation adjusted by the efficiency of immunoprecipitation was calculated. The average and standard deviations for two independent analyses are presented (*bottom panel*). *B*, PML acetylation is increased in response to TSA treatment. HeLa cells were transfected with indicated expression vectors and treated with or without 10 μM TSA for 4 h. PML acetylation was analyzed and presented as in *A*. *WB*, Western blotting.

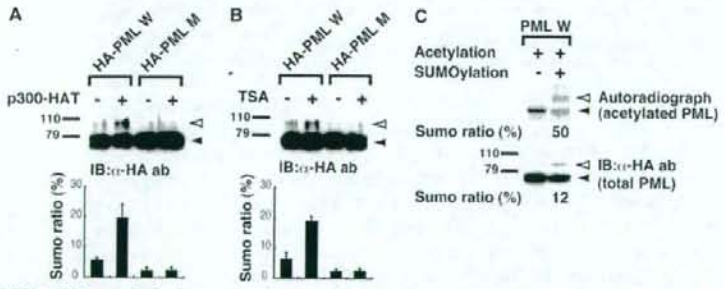

FIGURE 4. **PML acetylation is associated with enhanced sumoylation.** *A*, p300 coexpression enhances PML sumoylation. HeLa cells were transfected with the indicated expression vectors with cotransfection of those for SUMO and Ubc9. The cell lysates were subjected to SDS-PAGE followed by immunoblotting (*IB*) with anti-HA antibody (*ab*). The positions of sumoylated PML detected as an upper shifted band and nonsumoylated PML are indicated by *white* and *black arrowheads*, respectively. The ratios of sumoylated PML to total (sumoylated and unsumoylated PML) were calculated (SUMO ratio) and presented as bar charts. *B*, PML sumoylation increases in response to TSA treatment. PML sumoylation was examined as in *A* except that cells were treated with 10 μM TSA for 4 h instead of cotransfection of p300-HAT. *C*, acetylated PML is preferentially sumoylated *in vitro*. HA-tagged PML protein synthesized *in vitro* was immunoprecipitated with anti-HA antibody and incubated with p300-HAT and [^{14}C]acetyl-CoA as in Fig. 2*A*. The protein was subjected to an *in vitro* sumoylation assay and SDS-PAGE and transferred to a polyvinylidene difluoride membrane. Sumoylation of total (acetylated and nonacetylated) PML was visualized by IB with anti-HA antibody (*lower panel*). The same membrane was also subjected to an autoradiography to visualize sumoylation of acetylated PML (*upper panel*). Sumoylated and nonsumoylated PML are indicated as in *A*. SUMO ratio in each panel were calculated and presented at the *bottom*.

DISCUSSION

The data presented here demonstrate that acetylation of PML may enhance its sumoylation and play an important role in the control of PML-dependent apoptosis in response to TSA exposure. Sumoylation of PML is necessary for NB formation (5, 10), and the apoptotic effects of PML may be dependent on NB formation (see Introduction). Given our findings that PML acetylation is associated with increased PML sumoylation, this sumoylation-dependent NB formation may represent one of the mechanisms by which PML acetylation can enhance apoptosis. This hypothesis is supported by our findings that coexpression of SUMO and Ubc9 enhances PML-dependent apoptosis by TSA, that acetylation-defective mutants of PML exhibit defects in sumoylation and apoptosis in response to TSA treatment, and that a sumoylation-impaired PML mutant (PML-3K) is